HHS Public Access

Author manuscript

Nat Microbiol. Author manuscript; available in PMC 2023 July 05.

Published in final edited form as:

Nat Microbiol. 2023 January ; 8(1): 28–39. doi:10.1038/s41564-022-01282-x.

CanB is a metabolic mediator of antibiotic resistance in *Neisseria gonorrhoeae*

Daniel H.F. Rubin[1], **Kevin C. Ma**[1], **Kathleen A. Westervelt**[1], **Karthik Hullahalli**[2,3], **Matthew K. Waldor**[1,2,3], **Yonatan H. Grad**[1,2]

[1]Department of Immunology and Infectious Diseases, Harvard T.H. Chan School of Public Health, Boston, MA, USA

[2]Division of Infectious Diseases, Brigham and Women's Hospital, Harvard Medical School, Boston, MA, USA

[3]Department of Microbiology, Harvard Medical School, Boston, MA, USA

Abstract

The evolution of the obligate human pathogen *Neisseria gonorrhoeae* has been shaped by selective pressures from diverse host niche environments as well as antibiotics. The varying prevalence of antibiotic resistance across *N. gonorrhoeae* lineages suggests that underlying metabolic differences may influence the likelihood of acquisition of specific resistance mutations. We hypothesized that the requirement for supplemental CO_2, present in approximately half of isolates, reflects one such example of metabolic variation. Here, using a genome-wide association study and experimental investigations, we show that CO_2-dependence is attributable to a single substitution in a β-carbonic anhydrase, CanB. CanB^{19E} is necessary and sufficient for growth in the absence of CO_2, and the hypomorphic CanB^{19G} variant confers CO_2-dependence. Furthermore, ciprofloxacin resistance is correlated with CanB^{19G} in clinical isolates, and the presence of CanB^{19G} increases the likelihood of acquisition of ciprofloxacin resistance. Together, our results suggest that metabolic variation has impacted the acquisition of fluoroquinolone resistance.

Corresponding author Yonatan Grad, Department of Immunology and Infectious Diseases, Harvard T.H. Chan School of Public Health, 665 Huntington Ave. Building 1, Room 715, Boston, MA, 02115, ygrad@hsph.harvard.edu; tel: 617-432-2275.

Author contributions

DHFR and KCM performed the GWAS and statistical analyses. DHFR and KAW performed the anaerobic experiments. DHFR and KH performed the macrophage experiments. The remainder of the experimental work was performed by DHFR. All authors (DHFR, KCM, KAW, KH, MKW, YHG) contributed to data interpretation. YHG supervised and managed the study. DHFR and YHG wrote the manuscript. All authors reviewed and edited the final manuscript. All authors were responsible for the decision to submit for publication.

Code Availability

Code used in this current study has been previously published.[68]

Biological Materials

All biological materials used in this study, including new constructs, are available from the corresponding author on reasonable request.

Competing interests

YHG is on the Scientific advisory board of Day Zero Diagnostics and consulted for GSK. YHG has received funding from Merck and Pfizer. None of these competing interests has a bearing on this project. The remainder of the authors declare no competing interests.

Introduction

Neisseria gonorrhoeae is the cause of the highly prevalent sexually transmitted infection gonorrhea, with an estimated 87 million new cases worldwide in 2016[1]. *N. gonorrhoeae* can infect multiple anatomical sites, including the urethra, cervix, rectum, and oropharynx[2], and therefore interacts with and adapts to host immune and site-specific pressures[3,4]. In addition to these pressures, the evolution of the gonococcus has been shaped by antibiotics. *N. gonorrhoeae* has acquired resistance to every first-line antibiotic used to treat it[5], including the fluoroquinolone ciprofloxacin—with resistance around 35% in the US and >90% in several countries[6–9]—and the current first-line therapy, the extended spectrum cephalosporin ceftriaxone[10,11].

Antibiotic resistance varies across the phylogenetic tree, with some lineages displaying more resistance than others, though the reasons for these differences are not known. *N. gonorrhoeae* has two major lineages, distinguished by sexual networks and levels of antibiotic resistance: lineage A, associated with men-who-have-sex-with-men and high levels of antibiotic resistance, and lineage B, associated with heterosexuals and lower levels of resistance[12] (Fig. 1A).

One hypothesis to explain the phylogenetic variation in resistance is that lineages may be subject to demographically or geographically variable antibiotic pressures. The overrepresentation of specific transmission networks based on sexual behavior within lineages lends support to this hypothesis[12], but the rapid global spread of *N. gonorrhoeae* and the extensive bridging across sexual networks argue against it[13,14]. As metabolic factors can contribute to resistance[15] and metabolic environment affects antibiotic resistance acquisition[16], we hypothesized that metabolic variation may be one factor contributing to why some lineages more readily acquire resistance.

One metabolic factor with known variation is CO_2-dependence. In a clinical setting, protocols recommend growing *N. gonorrhoeae* in the presence of 5% supplemental CO_2[17]. However, only around half of clinical isolates require CO_2 for growth[18], suggesting that that there may be a genetic basis for this dependency. Here, we found that CO_2-dependence in *N. gonorrhoeae* is driven by a single mutation in the *N, gonorrhoeae* β-carbonic anhydrase, CanB, that this mutation is associated with resistance to ciprofloxacin in clinical isolates, and that this mutation compensates for fitness costs incurred by gyrase mutations that confer ciprofloxacin resistance.

Results

A single mutation in CanB is necessary and sufficient for CO_2-dependence in N. gonorrhoeae

We first investigated the mechanism of CO_2-dependence using a genome-wide association study (GWAS). To generate phenotypes for GWAS, clinical and laboratory strains of *N. gonorrhoeae* were assessed for growth in the presence and absence of supplemental CO_2. The GWAS revealed a significant association with a single genomic site, a missense mutation in *ngo2079* (Fig. 1B). In a parallel unbiased method, genomic DNA from FA6140,

an *N. gonorrhoeae* strain that does not depend on supplemental CO_2, was used to transform FA19, a lab isolate that requires supplemental CO_2 (Extended Data 1A). Transformants that grew in the absence of supplemental CO_2 had acquired multiple SNPs in the region of *ngo2079* (Extended Data 1B). As the SNP identified in the GWAS was also present in the undirected transformant, we proceeded with further investigation of the mutation in *ngo2079*.

The *ngo2079* c.56G→A SNP encodes a G→E mutation at amino acid 19 of NGO2079, a β-carbonic anhydrase. *N. gonorrhoeae* contains two additional carbonic anhydrases: a well-characterized essential periplasmic α-carbonic anhydrase[19–21] and a putative nonessential cytosolic ɣ-carbonic anhydrase[22]. All carbonic anhydrases catalyze the conversion of H_2O and gaseous CO_2 to aqueous bicarbonate. Aqueous bicarbonate is then used as a carbon building block in multiple pathways within the cell, including the synthesis of TCA cycle components, nucleotides, and phospholipids[23] (Extended Data 1C). As *ngo2079* is the sole predicted *N. gonorrhoeae* β-carbonic anhydrase, we named this gene *canB* to parallel the corresponding carbonic anhydrase *can* in *E. coli*. The SNP is located outside of the highly conserved carbonic anhydrase domain (Extended Data 1D) and does not appear to be within a signal sequence domain by SignalP[24]. Structures from Alphafold[25] indicate that the variant amino acid lies between two N-terminal alpha-helices, but it does not appear at the dimerization interface or the characterized active site (Extended Data 1E).

We validated our GWAS results by introducing the CanB variants into *N. gonorrhoeae*. Replacement by kanamycin co-selection of the $CanB^{19E}$ in FA1090 with $CanB^{19G}$ and of the $CanB^{19G}$ in FA19 with $CanB^{19E}$ showed that dependence on supplemental CO_2 was attributable to $CanB^{19G}$ (Fig. 1C), while similar results for single point mutants in 28BL (19E→G) and FA19 (19G→E) (Fig. 1D) support this idea. These results indicate that $CanB^{19E}$ is both necessary and sufficient for growth in the absence of supplemental CO_2. The concentration of CO_2 that differentiates this dependency is between atmospheric (~410 ppm) and 0.1% CO_2 (1000 ppm) (Extended Data 2A), slightly lower than has been found in other bacteria[26] and considerably below the 5% CO_2 standardly used in *N. gonorrhoeae* growth protocols[27].

$CanB^{19G}$, the allele that confers CO_2-dependence, appears to have arisen multiple times in *N. gonorrhoeae*, whereas genomes from *Neisseria spp.* and other closely related bacteria encode only $CanB^{19E}$ (Fig. 1E). Analysis of the PubMLST database of more than 36,000 *Neisseria spp.* genomes showed that only one non-gonococcal *Neisseria* isolate carries $CanB^{19G}$, a urethral isolate of *N. meningitidis* (PubMLST id: 82427) that appears to have a acquired the *canB* region from *N. gonorrhoeae* (100% identity to sequenced *N. gonorrhoeae* isolates). Within *N. gonorrhoeae*, ~50% of sequenced isolates from across the phylogenetic tree have $CanB^{19G}$ (Fig. 1A, E). The proportion of sequenced isolates with $CanB^{19G}$ has remained relatively stable at ~50% during last twenty years (Extended Data 1F), though this allele may have been less common in the pre-antibiotic era of the 1930s (1/11 (9%) of pre-1930 *N. gonorrhoeae* isolates from the Pub-MLST database).

Although $CanB^{19E}$ provides a growth advantage in the absence of supplemental CO_2, the growth of FA19 $CanB^{19G}$ and $CanB^{G19E}$ in the presence of supplemental CO_2 was

indistinguishable and independent of inoculum size (Fig. 1F, left). Furthermore, in the presence of CO_2, kanamycin-labeled CanB isogenic FA19 strains remained at similar proportions in competition over time as compared to the input (Extended Data 2B). The CanB^{19G} variant, therefore, does not confer a general fitness defect but a specific growth disadvantage in the absence of CO_2. As shown in Fig. 1F, right, this disadvantage is concentration-dependent and is exacerbated at lower starting inocula. Although FA19 CanB^{19E} is able to grow at all starting CO_2 concentrations, both strains have a substantially longer lag phase in the absence of CO_2, suggesting that intracellular bicarbonate plays a critical role in lag phase, similar to *N. meningitidis*[28]. This competitive disadvantage is not rescued by extracellular sodium bicarbonate or oxaloacetate, a downstream product of intracellular bicarbonate (Extended Data 2C). Thus, in contrast to many bacteria that are able to acquire bicarbonate from the environment via inorganic carbon transporters[29], *N. gonorrhoeae* does not appear to have a CO_2-concentrating mechanism apart from cytosolic carbonic anhydrases, explaining why exogenous bicarbonate does not rescue the competition defect. Supplementation with metabolites downstream of intracellular bicarbonate (Extended Data 1D), such as pyruvate, sub-minimum inhibitory concentration (MIC) palmitic acid, and pyrimidines were also unable to rescue this defect (Extended Data 2D).

CanB^{19G} has reduced enzymatic activity compared to CanB^{19E}

E. coli MG1655 was used to compare the activity of the CanB variants. Deletion of one of the two endogenous *E. coli* β-carbonic anhydrases, *can*, rendered MG1655 capnophilic and dependent on supplemental CO_2 (Fig. 2A, top two quadrants). Complementation with IPTG-inducible *N. gonorrhoeae* CanB variants restored growth in the absence of supplemental CO_2. However, lower concentrations of IPTG were required for complementation with CanB^{19E} versus CanB^{19G} (Fig. 2A, lower two quadrants), even though the abundance of CanB^{19E} and CanB^{19G} were similar at equivalent levels of induction (Extended Data 2E), suggesting that CanB^{19G} retains some enzymatic activity but does not restore growth as efficiently as CanB^{19E}.

Since CanB^{19G} is a hypomorph, we hypothesized that the CanB variants result in altered gonococcal physiology. At pH 4.5, an acidic condition similar to healthy vaginal pH[30], FA19 CanB^{19G} died more quickly than the isogenic FA19 CanB^{19E} (Fig. 2B, C), consistent with the finding that, in the absence of supplemental CO_2, FA19 CanB^{19G} is less able to buffer intracellular pH (Fig. 2D). The CanB^{19E} survival advantage at low pH did not extend, however, to intracellular survival within immortalized macrophages (Extended Data 3A). At higher pH and in aerobic conditions, neither the CanB^{19E} or CanB^{19G} variant displayed a substantial advantage (Extended Data 2B, Extended Data 3B). In contrast, under anaerobic conditions, FA19 CanB^{19E} had a distinct growth advantage in competition (Fig. 2E). Our data thus show that the CanB^{19E} allele provides an advantage at low pH and under anaerobic conditions, suggesting that CanB^{19E} may allow for buffering in the acidic vaginal environment.

CanB^{19G} is associated with ciprofloxacin resistance in clinical isolates

Carbonic anhydrases have been previously shown to be targets of sulfa antibiotics[21] and to mediate natural competence in *N. meningitidis*[31]. Sulfa antibiotics were one of the first

antibiotics to be used to treat gonorrhea[32] and primarily target dihydropteroate synthase in the folate synthesis pathway. Both CanB variants had similar sulfamethoxazole MICs across two genetic backgrounds. Similarly, the FA19 CanB isogenic pair had similar trimethoprim/sulfamethoxazole MICs, though in 28BL, there was a modest twofold increase in the CanB^{E19G} strain (Extended Data 4A). Furthermore, MG1655Δ*can* complemented with CanB^{19G} or CanB^{19E} also had similar sulfamethoxazole MICs (Extended Data 4B). The CanB variants therefore do not have different susceptibility to sulfa antibiotics. With respect to competence, while a *canB* knockout was dependent on supplemental CO_2 (Extended Data 5A), both the wild-type and knockout had the same level of natural competence, as measured by the introduction of a single SNP in *gyrB* conferring nalidixic acid resistance (Extended Data 5B). Similarly, competence was not associated with the CanB isogenic pairs of FA19 and 28BL (Extended Data 5B), though there were small differences in competence likely due to increased piliation from strain construction. Furthermore, there was no difference in nalidixic acid susceptibility at baseline between the FA19 isogenic strains (Extended Data 4C), suggesting that the competence assay was not biased by underlying changes in nalidixic acid resistance. Finally, as an additional control, introduction of a kanamycin cassette led to similar transformation efficiencies between isogenic pairs (Extended data 5C). Thus, selection for CanB variants does not appear to be driven by associations with sulfa susceptibility or natural competence.

We instead hypothesized that genomic and associated metabolic variation could modify the likelihoods of acquiring and maintaining resistance. Support for this idea comes from previous research showing that intracellular metabolite perturbations can shape the likelihood of developing resistance[16,33]. To begin to address whether the CanB variants have shifted the evolutionary landscape of *N. gonorrhoeae* antibiotic resistance, we analyzed whether the variants are associated with antibiotic resistance on the population level. We found that the CanB^{19G} variant is associated with >4-fold higher MICs for ciprofloxacin (average $\log_2$ MIC 0.43 vs. 0.10 μg/mL) (Fig. 3A), whereas MICS for azithromycin (0.32 μg/mL vs. 0.24 μg/mL), penicillin (0.41 vs. 0.70 μg/mL), and ceftriaxone (.0093 μg/mL vs. .013 μg/mL) did not differ (Extended Data 6A). CanB^{19G} is also associated with the most common resistance determinant for ciprofloxacin, GyrA^{91F}, as 52.3% of CanB^{19G} isolates have GyrA^{91F}, as compared to only 30.4% of CanB^{19E} isolates ($p<0.0001$, Pearson's chi-square) (Fig. 3B). This relationship holds true across years, as the proportion of GyrA^{91F} and CanB^{19G} isolates per year in the United States have tracked closely since 2000 (Fig. 3C). On a country-by-country level, isolates with CanB^{19G} have a comparatively higher ciprofloxacin MIC (Extended Data 6B), indicating that the association is true across datasets and geography. One possible explanation is that CanB^{19G} directly increases ciprofloxacin resistance. However, the isogenic CanB FA19 strains have comparable levels of resistance to ciprofloxacin (Extended Data 4C).

CanB^{19G} compensates for gyrase mutation-related fitness costs

We reasoned that there were multiple potential mechanistic explanations for the differences in ciprofloxacin associated with the CanB^{19G} and CanB^{19E} variant strains. The first is that CanB^{19G} has a higher mutation rate, manifesting as a higher rate of resistance to all antibiotics and therefore leading to more ciprofloxacin resistance. This does not appear

to be the case, since FA19 CanB^{19E} had a modestly higher mutation rate to rifampin, an antibiotic that targets RNA polymerase, by fluctuation assay (Extended Data 6C, D). There was additionally no difference in killing by ciprofloxacin for either strain, suggesting that the population-level difference in ciprofloxacin resistance between the strains is not due to differential viability in the presence of drug (Extended Data 7A).

A further possibility is that the CanB^{19G} strains have an increased ability to tolerate *gyrA* mutations. If this were true, we would expect that CanB^{19E} *gyrA* mutants would have a relative competitive disadvantage compared to the parental strains. To investigate this possibility, we generated GyrA^{91F} and GyrA$^{91F/95G}$ mutants in both FA19 CanB backgrounds. For both the GyrA^{91F} and GyrA$^{91F/95G}$ mutants, the CanB^{19E} strain was significantly disadvantaged against the parental strain (Fig. 4A). In monoculture, FA19 CanB^{19E} GyrA$^{91F/95G}$ also grew significantly slower than FA19 CanB^{19G} GyrA$^{91F/95G}$ (Fig. 4B, Extended Data 7B), as did the equivalent mutants in the 28BL background (Extended Data 7C). We generated spontaneous ciprofloxacin resistant mutants, all of which bore GyrA^{95} variants seen in clinical isolates (Extended Data 4D). The ciprofloxacin-resistant FA19 CanB^{19G} strains competed better than ciprofloxacin-resistant CanB^{19E} strains against the susceptible parental strains (Extended Data 7D) and showed faster growth in monoculture (Extended Data 7E). Furthermore, acquisition of the specific GyrA$^{91F/95G}$ allele was not different in a natural transformation experiment (Extended Data 5D). Importantly, this experiment was performed on a limited time-scale, minimizing any differences in fitness between the strains. Taken together, these results suggest that the increased rate of acquisition of ciprofloxacin resistance in the CanB^{19G} background is due to its higher relative fitness in the background of gyrase mutations. This finding also suggests that, particularly with the recent expansion of GyrA^{91F} isolates (Fig. 3C), there may be pressure in the *gyrA* mutant background to select for the CanB^{19G} variant. Thus, while *canB* variation is present in the *N. gonorrhoeae* population prior to the introduction of fluoroquinolones, we cannot rule out that CanB^{19G} may also represent a compensatory mutation acquired following *gyrA* mutation in at least some cases.

To investigate the mechanism of compensation and the fitness effects of GyrA in the FA19 CanB^{19E} background, we performed RNA-sequencing (RNA-seq) on FA19 CanB^{19G}, FA19 CanB^{19E}, and FA19 CanB^{19E} GyrA^{91F} growing in log-phase liquid culture with 5% CO_2 and focused on transcripts that were differentially regulated between FA19 CanB^{19E} and FA19 CanB^{19E} GyrA^{91F}, but not differentially expressed between FA19 CanB^{19G} and FA19 CanB^{19E}. We identified 151 such transcripts, including the downregulation in FA19 CanB^{19E} GyrA^{91F} of *purK*, encoding an N5-carboxyaminoimidazole ribonucleotide synthase involved in purine synthesis (Supp. Table 1, Fig. 4C).

Based on this finding, we hypothesized that purine availability modulates fitness in a manner dependent on carbonic anhydrase and gyrase. Purine nucleosides, including inosine (Fig. 4D), adenosine, and guanosine (Extended Data 7F) were sufficient to rescue the growth defect of FA19 CanB^{19E} GyrA^{91F} in competition with FA19 CanB^{19E}. In contrast, supplementation with pyrimidines had no effect on competition between the two strains (Extended Data 7F). Furthermore, purine supplementation had no effect on competition between FA19 CanB^{19G} GyrA^{91F} and FA19 CanB^{19G} (Extended Data 7G). Thus, purine

nucleosides rescued the growth defect conferred by GyrA^{91F} in the CanB^{19E} background. CanB^{19E} also shows lineage-specific background dependence, as the alleviation of CO_2-dependence in clinical isolate NY0195 requires further introduction of AasN^{Q321E}, a mutation in an acyl-ACP synthetase involved in fatty acid uptake[34] (Extended Data 8A). The AasN^{321Q} variant is restricted to a single lineage that carries the ceftriaxone-resistance determining PenA34 allele (Extended Data 8B), suggesting further complex connections between central metabolism and antibiotic resistance.

Discussion

Collectively, our findings suggest that CanB represents a metabolic mediator of drug resistance acquisition in *N. gonorrhoeae*. CanB^{19G} is present in about half of clinical isolates of *N. gonorrhoeae* and explains the growth requirement for supplemental CO_2; in contrast, isolates with CanB^{19E} can grow without this requirement. Although *canB* is not essential for *in vitro* growth (Extended Data 5A), we observed no evidence of premature stop codons in a collection of >16,000 genomes from clinical isolates, indicating its important role *in vivo*. The hypomorphic CanB^{19G} allele distinguishes *N. gonorrhoeae* from the other *Neisseriae*, which primarily inhabit the oropharyngeal niche as commensals, and it is also found in *N. gonorrhoeae* specimens pre-dating the introduction of antibiotics, together suggesting it reflects adaptation to the urogenital niche or sexual transmission.

The two CanB alleles generated distinct metabolic landscapes on which subsequent pressures acted, as CanB^{19G} facilitates the acquisition of ciprofloxacin resistance when compared with CanB^{19E}, a process mediated via purine availability. There are three possible explanations for the relationship among purines, GyrA mutations, and CanB mutations. The first is that changes in supercoiling from gyrase mutations may lead directly to transcriptional differences of purine synthesis genes such as *purK* and thereby cause a purine deficiency and decreased fitness. A second possibility is that gyrase mutations indirectly drive changes in nucleotide pools via changes in mutational burden, leading to a secondary effect on purine synthesis. This hypothesis is supported by the finding that the mismatch repair enzyme MutS is upregulated in the GyrA^{91F} mutant (Fig. 4C). A third possibility is that the gyrase mutant strains are not purine deficient, but instead purine supplementation has other effects on cellular metabolism, such as aerobic respiration[35], supported by the observation that NADH dehydrogenase components are downregulated in this mutant (Fig. 4C). As PurK is bicarbonate-dependent[36], any of these three mechanisms would be consistent with a complex interaction between *canB* and *gyrA* in *N. gonorrhoeae*. Future work will be needed to elucidate how gyrase mutations alter the metabolic landscape of the cell.

CanB^{19G} is therefore an example of a widespread variant that facilitates acquisition of drug-specific resistance through shifts in the gonococcal metabolic landscape and without directly affecting drug susceptibility or tolerance. This work builds on research showing that gene interactions are critical in compensating for the fitness costs incurred by resistance mutations[37–40], shows how pre-existing genetic variation can modulate the emergence and spread of antibiotic resistance mutations, and expands on recent findings that mutations in metabolic genes can change the drug-specific resistance profile of clinical isolates[15]. By

showing how specific lineages are more likely to acquire specific resistance determinants, our work provides a new perspective for understanding the evolution of antibiotic resistance.

Methods

Bacterial strains, culture conditions, MIC measurements, and figure design

Strains, plasmids, and primers are presented in Supplementary Table 1[41–50]. *N. gonorrhoeae* was cultured on GCB agar (Difco) with Kellogg's supplements[51] (GCB-K) at 37°C. Strains were grown at concentrations of CO_2 as indicated. Antibiotic susceptibility testing was performed on GCB agar with Kellogg's supplements via Etest (BioMerieux (azithromycin, ciprofloxacin, benzylpenicillin, ceftriaxone, trimethoprim/sulfamethoxazole) or agar dilution (for trimethoprim and sulfamethoxazole). For plating efficiency experiments, we made serial dilutions, then plated in parallel on GCB agar with Kellogg's supplements. For anaerobic growth on solid medium, *N. gonorrhoeae* strains were first grown overnight on GCB agar with Kellogg's supplement and additional supplementation with 1.2 mM $NaNO_2$. Growth curves and competitions in liquid culture were performed in GCP medium (15 g/L proteose peptone 3 (ThermoFisher), 1 g/L soluble starch (ThermoFisher), 4 g/L K_2HPO_4, 1 g/L KH_2PO_4, 5 g/L NaCl)[27] with Kellogg's supplement and additional metabolite supplementation as shown in the figures. Doubling time was determined by linear regression on $\log_2$-transformed CFU/mL data from 2–10 hours. Supplementation with metabolites did not affect pH unless otherwise noted. Anaerobic conditions were ensured using an anerobic hood and a gas mix consisting of 80% N_2, 10% CO_2, and 10% H_2. Optical density was measured at 600 nm. *E. coli* strains were cultured in LB. Figures were designed in Prism (v4.7) (GraphPad) and Illustrator (v26.5) (Adobe). Extended Data Figure 1D was adapted from the "Lac operon" template," by BioRender.com (2022, retrieved from https://app.biorender.com/biorender-templates).

Genomics pipeline and GWAS

Genomic analysis was conducted as in published work[3]. Reads were downloaded from sources also described[3]. These reads were inspected using FastQC (v0.11.7) (https://www.bioinformatics.babraham.ac.uk/projects/fastqc/) and removed for poor base quality or if GC content was divergent from expected values (~52–54%). Reads were then mapped to the NCCP11945 genome (RefSeq accession: NC_011035.1) using BWA-MEM (v0.7.17-r1188)[52]. We deduplicated using Picard (v2.8.0) (https://github.com/broadinstitute/picard). Samples with <70% reads aligned or with less than 40% coverage were identified with BamQC in Qualimap (v2.2.1)[53] and discarded. Pilon (v1.16)[54] was used to call variants with a mindepth of 10 and a minmq of 20 and pseudogenomes were generated from Pilon VCFs by including all PASS sites and alternate alleles with AF>0.9, while all other sites were set to "N" and samples with >15% of sites called as missing were excluded. *De novo* assemblies were created using SPAdes (v3.12.0, with 8 threads, the --careful flag, and paired end reads where available)[55]. Contigs were then filtered for quality (coverage >10X, length >500 bp, total genome size ~2.0–2.3 Mbp). Assemblies were annotated using Prokka (v1.13)[56]. Core genes were clustered using Roary (v3.12, using flags -z -e -n -v -s -i 92)[57] and core intergenic regions were clustered using piggy (v1.2)[58]. Gubbins (v 2.3.4)[59] was then used to construct a recombination-corrected phylogeny with the aligned pseudogenomes and the

resulting phylogeny was visualized in iTOL (v6)[60]. Metadata, including year, resistance determinants, and available susceptibility data have been collected and published[3]. For country level data, isolates with MICs that were annotated as greater than or less than that value were set to that value.

For the determination of GWAS phenotypes, thirty strains of *N. gonorrhoeae* were streaked on GCB agar with Kellogg's supplements in the presence and absence of supplemental 5% CO_2. These plates were then scored on a binary phenotype of growth/no growth in the absence of CO_2. For the computational aspect of the regression-based GWAS, we used a linear mixed model with a random effect to control for possible confounding by population structure. This linear mixed-model GWAS was run using Pyseer (v1.2.0 with default allele frequency filters)[61] based on 57,691 unitigs generated from the genome assemblies using unitig-counter (https://github.com/johnlees/unitig-counter). The Gubbins recombination-corrected phylogeny was used to parameterize the population structure random effects model in Pyseer. The resulting unitigs were mapped to the WHO F strain reference genome (Genbank accession: GCA_900087635.2) edited to contain only one locus of 23S rRNA using BWA-MEM (modified parameters -B 2 and -O 3). Significant unitigs were annotated through Pyseer's annotation pipeline. Unitigs were then further analyzed in Geneious Prime (v2021.0, http://www.geneious.com). The pipeline was run using Anaconda (v2021.11) and Python (v3.10.0).

RNA-Sequencing (RNA-seq)

For RNA-sequencing, strains of interest as indicated in the text were grown overnight in duplicate at 37C with 5% CO2 on GCB-K agar. Streaks were then scraped into liquid GCP medium with Kellogg's supplement and diluted to an OD of 0.1, followed by incubation with shaking at 200 rpm in a 37C incubator with 5% CO2. After the culture reached an OD of 0.2, cultures were pelleted. RNA was purified using the Direct-zol RNA Miniprep Kit (Zymo Research) according to the manufacturer's instructions. RNAseq library prep was performed by SeqCenter (seqcenter.com). As per SeqCenter, the isolated RNA was treated with DNAse (Invitrogen), and libraries were prepped with the Ribo-Zero Plus kit (Illumina) using Stranded Total RNA Prep Ligation with 10bp IDT for Illumina indices. Sequencing was then performed using a NextSeq2000, producing 2×50bp reads. The resulting reads were then demultiplexed with bcl-convert (v3.9.3) (https://support.illumina.com/sequencing/sequencing_software/bcl-convert.html) followed by quality control and adapter trimming. The resulting demultiplexed reads were then then mapped to the FA19 genome using bowtie2 (v2.4.5)[62]. Mappings were used to generate a vcd to check for additional mutations using bcftools (v1.15)[63]; none of the isolates had additional mutations. Features were mapped to the annotated FA19 genome using FeatureCounts (from the Subread package, v2.0.3)[64]. Counts were compared using DeSeq2 (v3.15)[65]. Transcripts of interest were filtered by both having a $|l2fc| > 1$ and $p_{adj} < 0.01$ between FA19 $CanB^{19E}$ and FA19 $CanB^{19E}$ $GyrA^{91F}$, while also having a $|l2fc| < 1$ and $p_{adj} > 0.01$ between FA19 $CanB^{19G}$ and FA19 $CanB^{19E}$. Significance is determined by the Wald test with Benjamini-Hochberg correction for multiple comparisons using default settings via DeSeq2 (v3.15). Data were analyzed via Rstudio (v1.2.1335, rstudio.com).

Undirected transformation of N. gonorrhoeae and determination of CO_2-dependent plating efficiency

For identification of the genetic modulator of CO_2 dependence (determined to be NGO2079), the CO_2-dependent laboratory strain FA19 was transformed with genomic DNA from the laboratory strain FA1090, which is CO_2-independent. Similarly, for identification of an additional mediator of CO_2-dependency (determined to be *aasN*), clinical isolate NY0195 was transformed with genomic DNA from the clinical isolate GCGS0457 using the following procedure. Liquid transformations were performed according to previously published protocols[27,50]. Piliated *N. gonorrhoeae* were grown on GCB-K agar overnight. The colonies were then resuspended in GCP medium with Kellogg's supplement, 10 mM $MgCl_2$, and approximately 400 ng genomic DNA. These suspensions were incubated at 37°C for 10 minutes in the presence of 5% CO_2 then rescued on non-selective GCB-K agar for 4 hours at 37°C with 5% CO_2. The recovered transformants were then re-plated on GCB-K agar and incubated overnight at 37°C without supplemental CO_2. The process was carried out in parallel without gDNA as a control for spontaneous mutation. Finally, colonies were subcultured for further analysis. To determine capacity for natural competence, strains of *N. gonorrhoeae* were transformed with pSY6, a plasmid conferring an allele of GyrB that confers nalidixic acid resistance[66], pDR1, a plasmid conferring Kan^R(Supp. Table 1), or a PCR product containing the allele for $GyrA^{91F/95G}$ amplified using primers DR_380 and DR_383, conferring ciprofloxacin resistance. Finally, serial dilutions of the transformants and negative control were plated in parallel on GCB-K agar plus Kellogg's supplement either without antibiotics, with 1 μg/mL nalidixic acid, 50 μg/mL kanamycin, or 0.03 μg/mL ciprofloxacin.

To determine the plating efficiency in the presence and absence of CO_2, *N. gonorrhoeae* was streaked overnight on GCB-K agar at 37°C with 5% CO_2. The resulting streaks were then serially diluted in at least triplicate and plated on GCB-K agar, with parallel dilutions being grown in the presence and absence of 5% CO_2 at 37°C. Plating efficiency was defined as the quotient of CFUs in the absence of CO_2 and CFUs in the presence of CO_2.

Sequencing and structural prediction

Following undirected transformation, genomic DNA from transformants was isolated using the PureLink Genomic DNA Mini kit (Life Technologies). Genomic DNA libraries were prepared and sequenced by the Microbial Genome Sequencing Center (https://www.migscenter.com/) on a NextSeq 2000. Resulting paired-end reads were then merged with BBMerge (v38.84)[67] and trimmed with BBDuk (v1.0). Reads were then mapped to the parental genomic DNA assembly and variants predicted in Geneious 2021.0 using default settings. Signal sequences were predicted using SignalP 6.0[24] and dimeric structures were predicted using AlphaFold (via Colab, https://colab.research.google.com/github/deepmind/alphafold/blob/main/notebooks/AlphaFold.ipynb)[25].

The resulting structures were then visualized in PyMOL (v2.5) (https://pymol.org).

CanB variant composition within Neisseria

Variant composition within *Neisseria* and closely related species at NGO2079/NEIS2004 was aggregated from multiple sources, including a previously published set of 12,111 *N. gonorrhoeae* isolates[68], PubMLST (https://pubmlst.org/, using NEIS2004 as reference, to obtain variant composition from *N. meningitidis*, *N. polysaccharea*, *N. cinerea*, *N. subflava*, *N. mucosa*, *N. lactamica* strains) and blastp (https://blast.ncbi.nlm.nih.gov/, using NGO2079 from *N. gonorrhoeae* isolate FA1090 as query, to obtain variant composition from *N. sicca*, *B. denitrificans*, *N. elongata*, *E. corrodens*). Genomes from strains representing a diverse set of species, listed in Figure 1C, were assembled as above or downloaded from Genbank and annotated 23S rRNA sequences were extracted from each genome. Each genome contained only a single annotataed 23S rRNA or all annotated 23S rRNA sequences were identical. Finally, a phylogenetic tree was constructed from these 23S rRNA sequences using RAxML (v8, 100 replicates, GTRGAMMA nucleotide model, Rapid Bootstrapping algorithm)[69]. The resulting tree was visualized in iTOL.

Targeted transformation of CanB and AasN—A ~1 kb PCR fragment surrounding the specific SNP of interest in *canB* was amplified using the primer pair (DR_250/DR_251) (see Supplementary Table 1). For *aasN*, the specific SNP of interest in *aasN* was amplified using primer pair (DR_341/DR_342). CO_2-dependent strains were transformed with approximately 600 ng of resulting PCR product and transformants were selected for growth on the absence of CO_2 as above. For selection of CO_2-dependent transformants from CO_2-independent parental strains, liquid transformations were performed as above and colonies were plated overnight on non-selective GCB-K agar. Colonies were then replica plated onto GCB-K agar and grown in parallel in the presence and absence of 5% CO_2. Finally, colonies that appeared to have CO_2-dependence were subcultured for further analysis. Transformation reactions using the alternative *canB* variant were used as a negative control to account for spontaneous mutation. For kanamycin co-selection, pDR50/51 was constructed using the following primer pairs: (DR_343/DR_344), (DR_345/DR_346), (DR_347/DR_348), (DR_349/DR_350), and (DR_194/DR_195) using Gibson assembly[70]. Liquid transformations were then performed on the above, followed by selection on GCB-K agar supplemented with 70 μg/mL kanamycin. Transformations without DNA were used as negative controls. All transformants were then checked by Sanger sequencing.

To knockout CanB, pDR35 was constructed using the following primer pairs:(DR_266/DR_272), (DR_273/DR_274), (DR_275/DR_276), (DR_277/DR_271), and (DR_194/195) using Gibson assembly and transformed as above. Similarly, to knockout AasN, pDR46 was constructed using primer pairs (DR_359/DR_360), (DR_361/DR362), (DR_363/DR_364), and (DR_194/DR_195). pDR46 was then transformed into *N. gonorrhoeae* followed by selection on 8 μg/mL chloramphenicol in GCB-K agar and checked by Sanger sequencing. Finally, for complementation of AasN, pDR75, a kanamycin resistant derivative of pMR32 was cloned, using primer pairs (DR_214/DR_215), (DR_216/DR_217), and (DR_218/DR_219) and Gibson assembly. Complementation constructs pDR48 and pDR49 were then cloned from pDR75 using restriction enzyme cloning with PacI/XbaI and an insertion product amplified by primer pair (DR_341/DR_342). These products were transformed into

the knockout strains, followed by selection on GCB-K agar supplemented with 70 μg/mL kanamycin.

Competition of CanB variants

Both FA19 CanB^{19G} and CanB^{G19E} were transformed with pDR1, a kanamycin cassette derivative (constructed with primer pairs (DR_62/DR_63), (DR_64/DR_65), and (DR_66/DR_67)) of pKH37[41]. The resulting transformants were selected on GCB-K agar supplemented with 50 μg/mL kanamycin and the resulting transformants were checked by colony PCR using primer pair (DR_62/DR_63). During competition experiments, FA19 CanB^{19G} was grown at a 1:1 starting ratio with kanamycin-resistant FA19 CanB^{G19E}, while in parallel FA19 CanB^{G19E} was grown at a 1:1 starting ratio with kanamycin resistant FA19 CanB^{19G}. At each timepoint, cultures were serially diluted and plated on both GCB-K agar and GCB-K agar supplemented with 50 μg/mL kanamycin. Finally, dilutions on both plates were quantified and the proportion of kanamycin resistant bacteria was quantified at each timepoint.

pH or antibiotic kill curves and determination of intracellular pH

Strains were plated overnight on GCB-K agar then scraped after 16–20 hours into liquid GCP medium with Kellogg's supplement. The cells were spun down in a microcentrifuge (13,500 × g for one minute) then resuspended in GCP medium with Kellogg's supplement. Cells were then diluted to an optical density of 1.00 and incubated in either pH-adjusted GCP medium with Kellogg's supplement (or, if noted, Graver-Wade medium[71]) or GCP medium with the defined concentration of antibiotics and Kellogg's supplement at 37°C in the absence of CO_2 in triplicate.

Intracellular pH was determined by using the BCECF-AM dye (ThermoFisher). Strains of interest were grown overnight on GCB-K agar with Kellogg's supplements. After 16–20 hours, streaks were resuspended in liquid GCP medium with Kellogg's supplement and diluted to a starting OD of 0.2. These strains were then grown in parallel in the presence and absence of 5% supplemental CO_2 for four hours in triplicate. Cells were then washed in PBS, resuspended in PBS with 1 μg/mL BCECF-AM dye, and incubated for thirty minutes. Finally, cells were measured for excitation/emission at both 440nm/535nm and 485nm/535nm in a plate reader. The fluorescence at both excitation/emission wavelengths from a control with dye but no cells was then subtracted from the measured 440nm/535nm and 485nm/535nm values. Finally, as the 440nm/535nm value is a proxy for cell density, the final (485nm/535nm)/(440nm/535nm) ratio was compared to a normal curve created using laboratory strain FA19 in the presence of Graver-Wade medium at multiple pHs and in the presence of 30 μg/mL of the decoupler CCCP (Sigma).

Intracellular macrophage survival

RAW264 macrophages were plated overnight in a 12-well plate at ~1 million cells/well in DMEM with 4 mM L-glutamine, 1.25 mM sodium pyruvate, and 10% heat-inactivated FBS (ThermoFisher). Cells were then infected with the strains of interest at an MOI of ~100. The plate was then centrifuged at 500 x g for 4 minutes to promote adherence and was incubated for 1 hour at 37°C with 5% CO_2. Cells were then washed three times in DMEM and finally

replated in the supplemented DMEM with 100 μg/mL gentamicin. At 0, 1, 2, and 4 hours, three wells for each bacterial strain were resuspended in 300 mL of 0.01% Triton-X-100 in sterile PBS by vigorous pipetting. The Triton-X-100 solution was incubated for ten minutes then vortexed vigorously, followed by dilution plating on GCB-K agar to determine the total intracellular bacterial burden.

Knockout of can and complementation of CanB variants in E. coli

pDR55, a derivative of the *sacB* allelic exchange vector pRE107[44], was cloned with primer pairs (DR_404/DR_405), (DR_406/DR_407), (DR_408/DR_409), and (DR_410/DR_411), to insert into *can* and transformed into the *E. coli* λpir DAP auxotroph β2155. The plasmid was then conjugated into *E. coli* MG1655 by incubating the two *E. coli* strains together at a 1:1 ratio on LB with 0.3 mM DAP in the presence of 5% supplemental CO_2. The resulting transformants were then plated onto LB without DAP in the presence of 5% supplemental CO_2. Finally, the resulting transformants were checked by colony PCR using primer pair (DR_402/DR_403) for successful knockouts. The resulting strains were then transformed with pDR42 and pDR43, both derived from pMR33[42] using restriction-enzyme cloning with enzymes PacI/XbaI and *canB*-FLAG amplified with primer pair (DR_280/DR_306), as well as empty-vector pMR33 and selected on LB agar with 20 μg/mL chloramphenicol. Finally, these strains were assessed for growth in the presence and absence of CO_2 at different levels of IPTG induction.

Proteins were quantified by Western blot. Briefly, MG1655Δ*can*::pDR42/43 was grown overnight in LB with 20 μg/mL chloramphenicol and 5% CO_2 at 37°C. Each strain was then diluted to OD 0.01 and then grown in the presence of different levels of IPTG inducer. After 4 hours, 1.5 mL of each culture was centrifuged (20,000 x g for 3 minutes) and resuspended in lysis buffer (1% v/v Triton-X-100, 150 mM NaCl, 2 mM EDTA, 20 mM Tris-HCl pH 7.5, 1X v/v cOmplete protease inhibitor (Sigma). After 30 minutes of incubation at 4°C with agitation, lysed cells were centrifuged at 4°C (2,800 x g for 5 minutes). The resulting supernatant was used for further protein analysis. Whole cell extracts were electrophoresed on 4–12 μg/mL Tris-Glycine gels (Invitrogen) and transferred to a PVDF membrane with semi dry transfer. The membranes were then blocked in 5% milk, incubated with primary antibodies to G6PD (1:2500, AssayPro) and FLAG-tag (1:2500, ThermoFisher), then HRP-conjugated goat anti-rabbit secondary antibodies (1:5000, ThermoFisher). Finally, the membranes were visualized with Pierce ECL Western Blotting Substrate (ThermoFisher) and visualized by chemiluminescent and colorimetric imaging.

Fluctuation analysis and gyrase mutants

gyrA^{91F} and *gyrA*$^{91F/95G}$ alleles were amplified by PCR using primer pair (DR_380/DR_383) from clinical *N. gonorrhoeae* isolate NY0195. These alleles were then introduced into strains FA19 and 28BL using liquid transformation as described above and selected on GCB-K agar with .003 and .006 μg/mL ciprofloxacin respectively.

For fluctuation analysis, *N. gonorrhoeae* strains were first streaked overnight. The resulting streaks were then resuspended in liquid GCP with Kellogg's supplement, diluted to OD 0.1, then re-plated onto GCB-K agar with Kellogg's supplement and plated for CFUs

with 6 replicates. After 16–20 hours, each well was resuspended in 200 μl of liquid GCP and agitated with beads. From each well, 40 μl was plated onto overdried GCB-K agar with Kellogg's supplement and the antibiotic of interest. Colonies were then counted after 24 hours. Furthermore, six wells were used to determine the number of plated CFUs by serial dilution on nonselective GCB-K agar with Kellogg's supplement. Mutation rates were determined using the R package flan (v0.9, default conditions, plating efficiency 0.2)[72]. For generation of Cip^R mutants, we generated unique mutants using the same method as in the fluctuation assay with plating on GCB-K agar with 0.01 μg/mL ciprofloxacin, followed by Sanger sequencing to validate gyrase mutations.

Extended Data

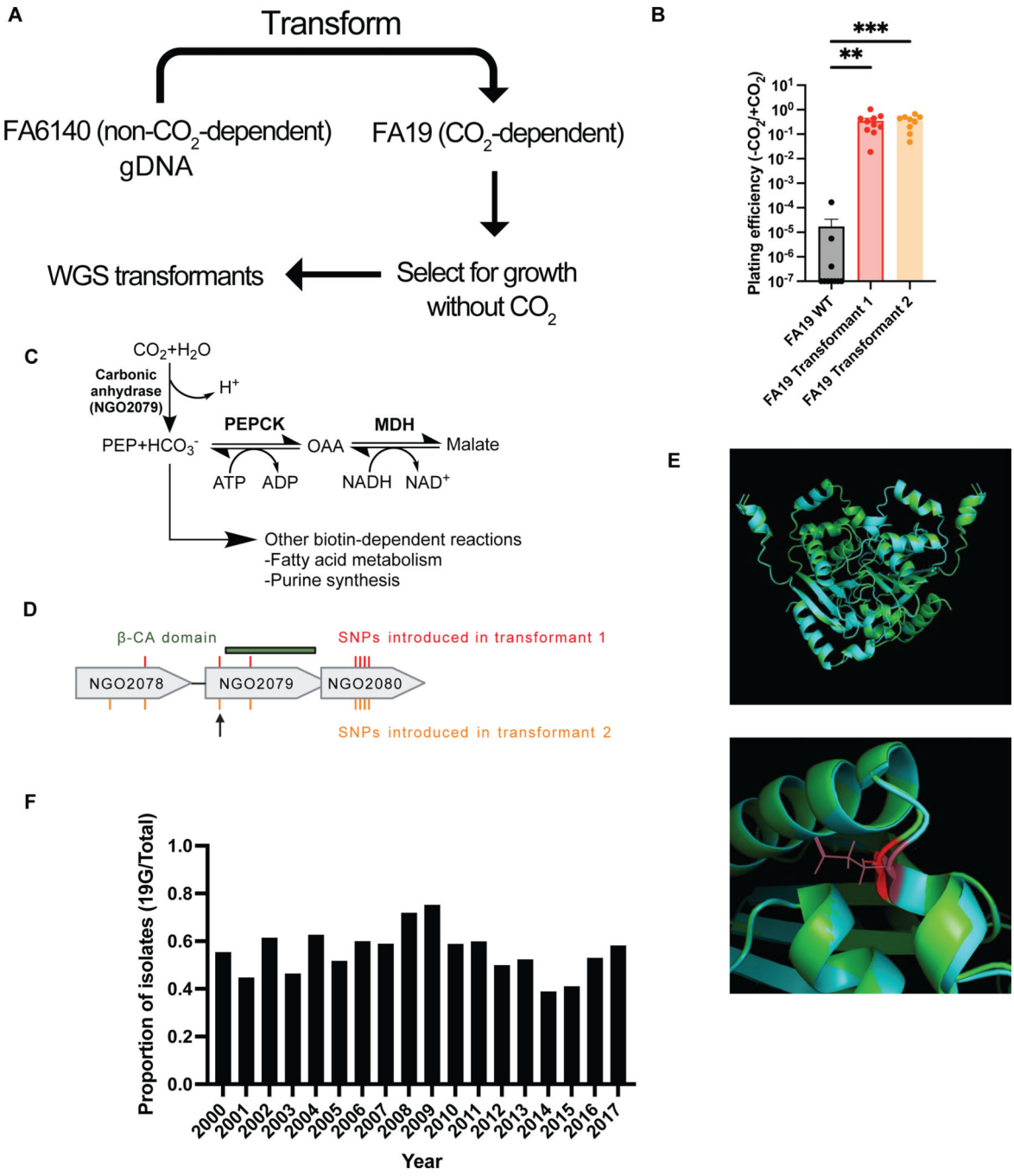

Extended Data Fig. 1.

(A) Schematic of undirected transformation of FA19 (parental CanB^{19G}) to identify causative factors for CO_2-dependence **(B)** Plating efficiency in the presence and absence of CO_2 following undirected transformation of gDNA from *N. gonorrhoeae* strain FA6140 into the *N. gonorrhoeae* lab strain FA19 (N = 10, 10, 9 from left to right from two independent experiments, error bars represent SEM). Significance (from left to right, p = 0.00018, p =

0.00028) determined by two-sided Mann-Whitney U test. **(C)** Putative reaction catalyzed by NGO2079/CanB and downstream metabolic products. **(D)** SNPs present in whole-genome sequencing of two transformants in **(B)**. Arrow indicates the SNP identified in Figure 1. **(E) (Top)** Alphafold predicted homodimeric structures of the CanB^{19E} variant (teal) and the CanB^{19G} variant (green). **(Bottom)** Magnified Alphafold predicted structures overlaying the glutamate (maroon) and glycine (red) at position 19. **(F)** Proportion of sequenced isolates by year with the CanB^{19G} variant. *p<0.05, **p<0.01, ***p<0.001

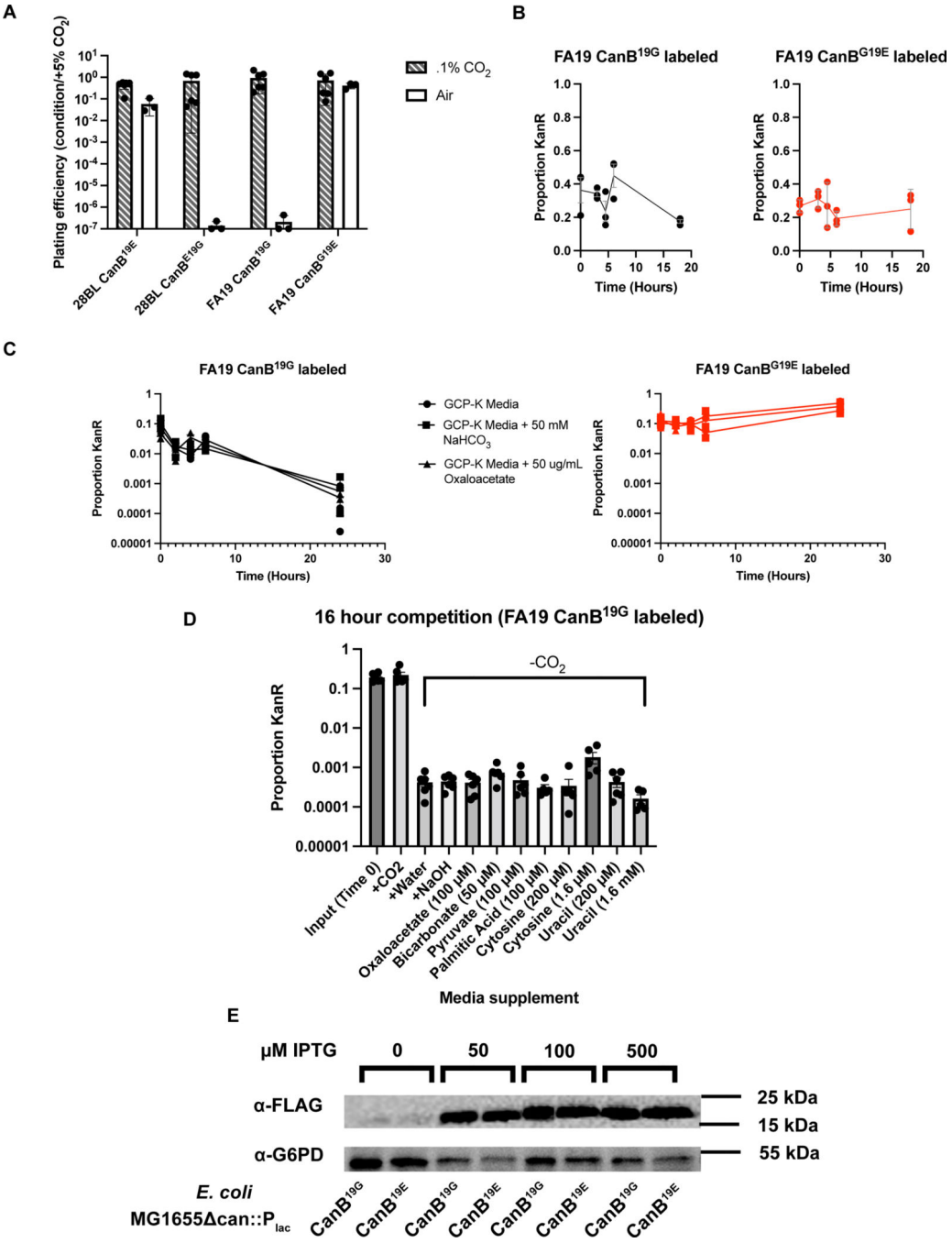

Extended Data Fig. 2.

(A) Plating efficiency at different CO_2 concentrations for *N. gonorrhoeae* strains 28BL (parental CanB^{19E}) and FA19 (parental CanB^{19G}) with isogenic CanB mutants (N = 6 for 0.1% CO_2, N = 3 for air, from two independent experiments, error bars represent SEM). **(B)** Competition experiment in the presence of CO_2 between FA19 CanB^{19G} and FA19 CanB^{E19G} with (**left**) the FA19 CanB^{19G} strain kanamycin-labeled and **(right)** the FA19 CanB^{E19G} kanamycin-labeled. The proportion of colony forming units (CFUs) that are kanamycin resistant is graphed against time (N=3, representative of two independent experiments, error bars represent SEM). **(C)** Similar to **(B)**, timecourse of competition between isogenic CanB FA19 strains in the presence of media supplementation and the absence of supplemental CO_2 (N=3, representative of two independent experiments, error bars represent SEM). **(D)** As in **(C)**, competition between unlabeled FA19 CanB^{G19E} and kanamycin-labeled FA19 CanB^{19G} with selected metabolite supplementation assayed at 16 hours in the absence of supplemental CO_2 (N=6, from two independent experiments, error bars represent SEM). (E) Western blot of *E. coli* MG1655*Δcan* complemented with IPTG-inducible CanB variants C-terminally FLAG-tagged with G6PD as loading control (representative of two independent experiments).

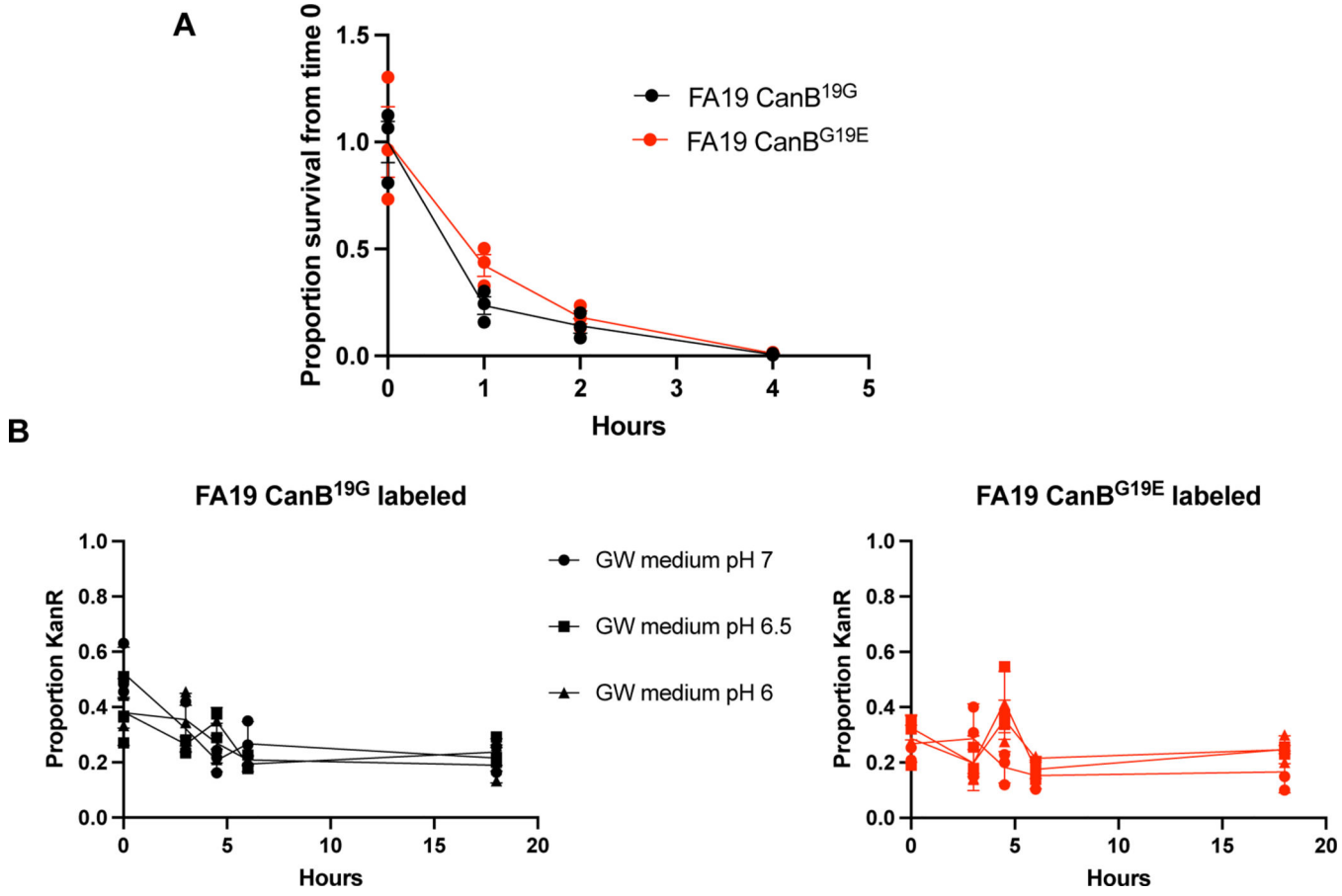

Extended Data Fig. 3.

The 19E variant of NGO2079 is not advantaged at moderately low pH or within macrophages. **(A)** Gentamicin intracellular protection assay in RAW 264.7 macrophages

as measured by CFUs (N=3/timepoint, representative of two independent experiments, error bars represent SEM). **(B)** Competition experiment as in Extended Data 2B in pH-adjusted Graver-Wade media (N=3, error bars represent SEM).

A

Drug MIC	FA19 CanB^{19G}	FA19 CanB^{G19E}
Sulfamethoxazole	**>256 μg/mL**	**>256 μg/mL**
TMP/SMX	**2 μg/mL**	**2 μg/mL**
Trimethoprim	**4 μg/mL**	**4 μg/mL**

Drug MIC	28BL CanB^{19E}	28BL CanB^{E19G}
Sulfamethoxazole	**>256 μg/mL**	**>256 μg/mL**
TMP/SMX	**12 μg/mL**	**6 μg/mL**
Trimethoprim	**4 μg/mL**	**4 μg/mL**

B

Drug MIC	MG1655Δ*can*::P_{lac}-CanB^{19G} + 50 μM IPTG	MG1655Δ*can*::P_{lac}-CanB^{19E} + 50 μM IPTG
Sulfamethoxazole	**256 μg/mL**	**256 μg/mL**

C

Drug	FA19 CanB^{19G}	FA19 CanB^{G19E}
Erythromycin	**.19 μg/mL**	**.19 μg/mL**
Chloramphenicol	**0.75 μg/mL**	**0.75 μg/mL**
Ciprofloxacin	**.003 μg/mL**	**.003 μg/mL**
Benzylpenicillin	**0.16 μg/mL**	**0.16 μg/mL**
Ceftriaxone	**<0.002 μg/mL**	**<0.002 μg/mL**
Nalidixic acid	**1 μg/mL**	**1 μg/mL**

D

CipR mutant	Mutation	Ciprofloxacin MIC (μg/mL)
FA19 CanB^{19G} Escapee 1	***gyrA*^{95N}**	**.032**
FA19 CanB^{19G} Escapee 2	***gyrA*^{95N}**	**.023**
FA19 CanB^{19G} Escapee 3	***gyrA*^{95G}**	**.032**
FA19 CanB^{G19E} Escapee 1	***gyrA*^{95N}**	**.032**
FA19 CanB^{G19E} Escapee 2	***gyrA*^{95N}**	**.047**
FA19 CanB^{G19E} Escapee 3	***gyrA*^{95N}**	**.032**
FA19 CanB^{19G} GyrA^{91F}	***gyrA*^{91F}**	**.047**
FA19 CanB^{G19E}GyrA^{91F}	***gyrA*^{91F}**	**.047**
FA19 CanB^{19G} GyrA$^{91F/95G}$	***gyrA*$^{91F/95G}$**	**.094**
FA19 CanB^{G9E} GyrA$^{91F/95G}$	***gyrA*$^{91F/95G}$**	**.094**

Extended Data Fig. 4.

(A) MICs for sulfamethoxazole, trimethoprim, and trimethoprim/sulfamethoxazole for the FA19 and 28BL pairs isogenic CanB variants. **(B)** Sulfamethoxazole susceptibility of MG1655Δ*can* complemented with isogenic CanB variants and induced with IPTG.

(C) MICs for clinically relevant antibiotics for FA19 CanB^{19G} and FA19 CanB^{E19G} as determined by E-test and agar dilution plating. **(D)** *gyrA* mutations for spontaneous ciprofloxacin escapees or clean mutants of FA19 CanB^{19G} and FA19 CanB^{19E}, along with associated ciprofloxacin MIC.

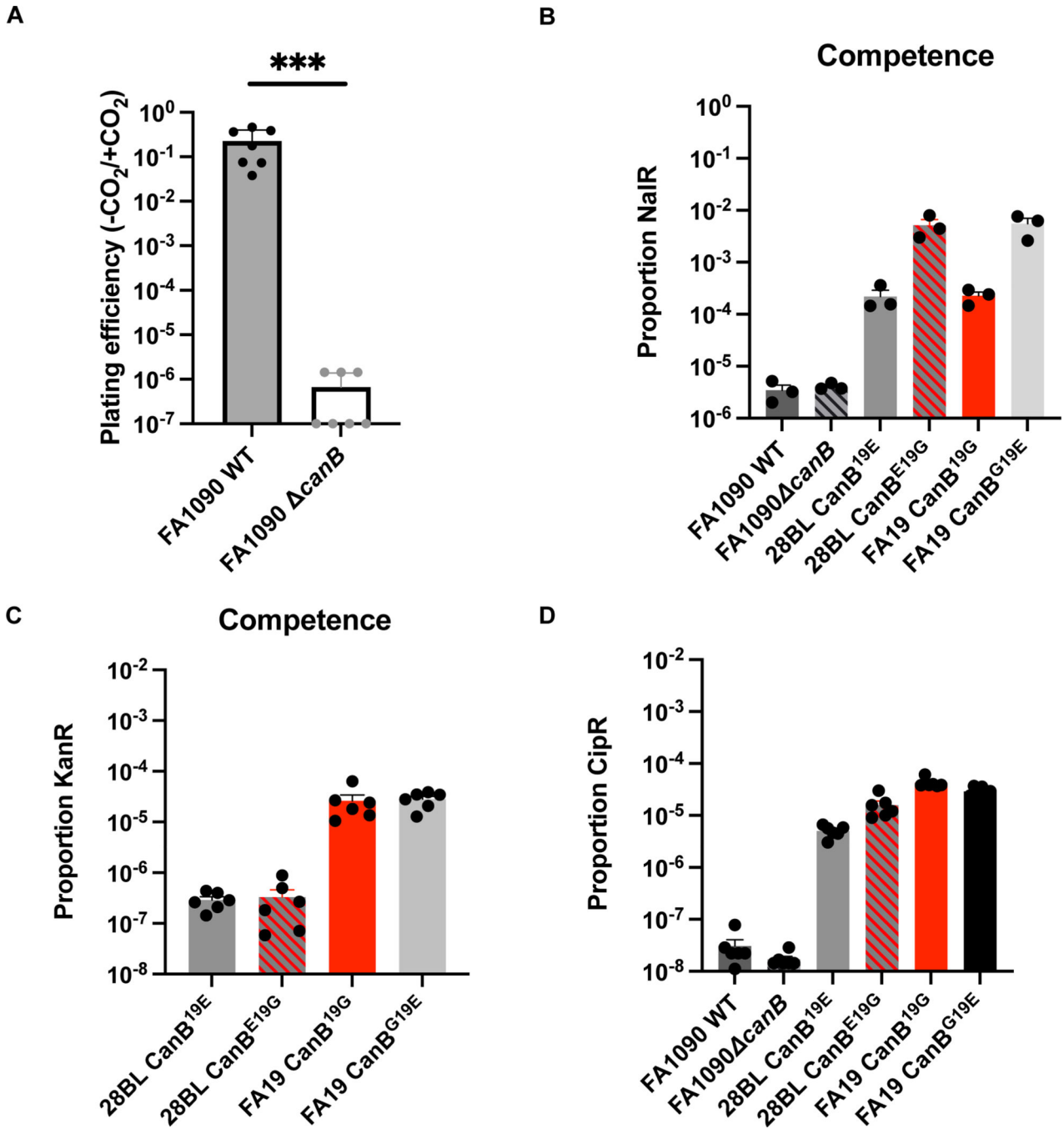

Extended Data Fig. 5.

Loss of CanB does not appear to confer a loss of natural competence. **(A)** Plating efficiency in the presence and absence of CO_2 for a knockout of *CanB* in the *N. gonorrhoeae* lab strain

FA1090 (N=6, from two independent experiments, error bars represent SEM). Significance (p=0.0006) by two-sided Mann-Whitney U. **(B)** Natural competence of strains of *N. gonorrhoeae* as measured by uptake of a nalidixic acid resistance-conferring integrating plasmid (N=3, representative of two independent experiments, error bars represent SEM). **(C and D)** As in **(B)**, natural competence as measured by **(C)** uptake of Kan^R-conferring plasmid DR1 and **(D)** a PCR product containing the allele encoding for $GyrA^{91F/95G}$ (N=6, representative of two independent experiments, error bars represent SEM). *p<0.05, **p<0.01, ***p<0.001

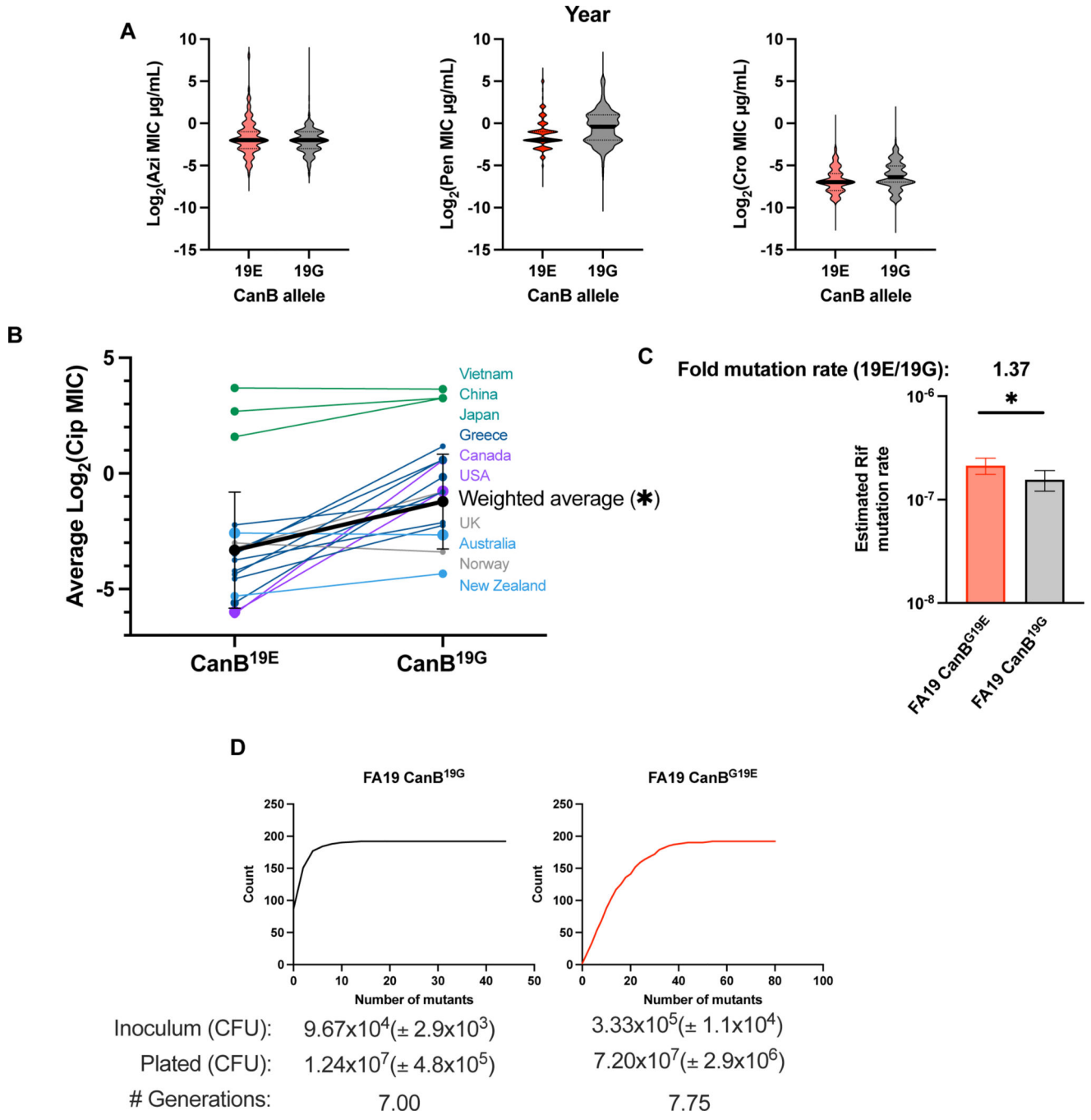

Extended Data Fig. 6.

(A) Violin plots of drug MICs for ~10,000 *N. gonorrhoeae* clinical isolates. Black bar represents median, dotted lines represent 25th/75th percentiles. **(B)** Average $\log_2$ of ciprofloxacin MIC in µg/mL by country and by allele of CanB. Weighted average of all datasets is represented by black dots/line. Size of data point represents size of dataset. Error bars represent standard deviation as determined by weighted variance. Significance (p = 0.0120) by unpaired two-sided t-test. **(C)** Calculated mutation rates of resistance acquisition for to rifampin by fluctuation analysis of isogenic CanB strains. (N=192,

representative of two independent experiments, error bars represent 95% confidence interval). Significance (p=0.029) by unpaired two-sided t-test (N=192, representative of two independent experiments, error bars represent SD). **(D)** Cumulative distribution of mutants in experiments in **(C)** along with data on the inoculum size and final population size. *p<0.05, **p<0.01, ***p<0.001

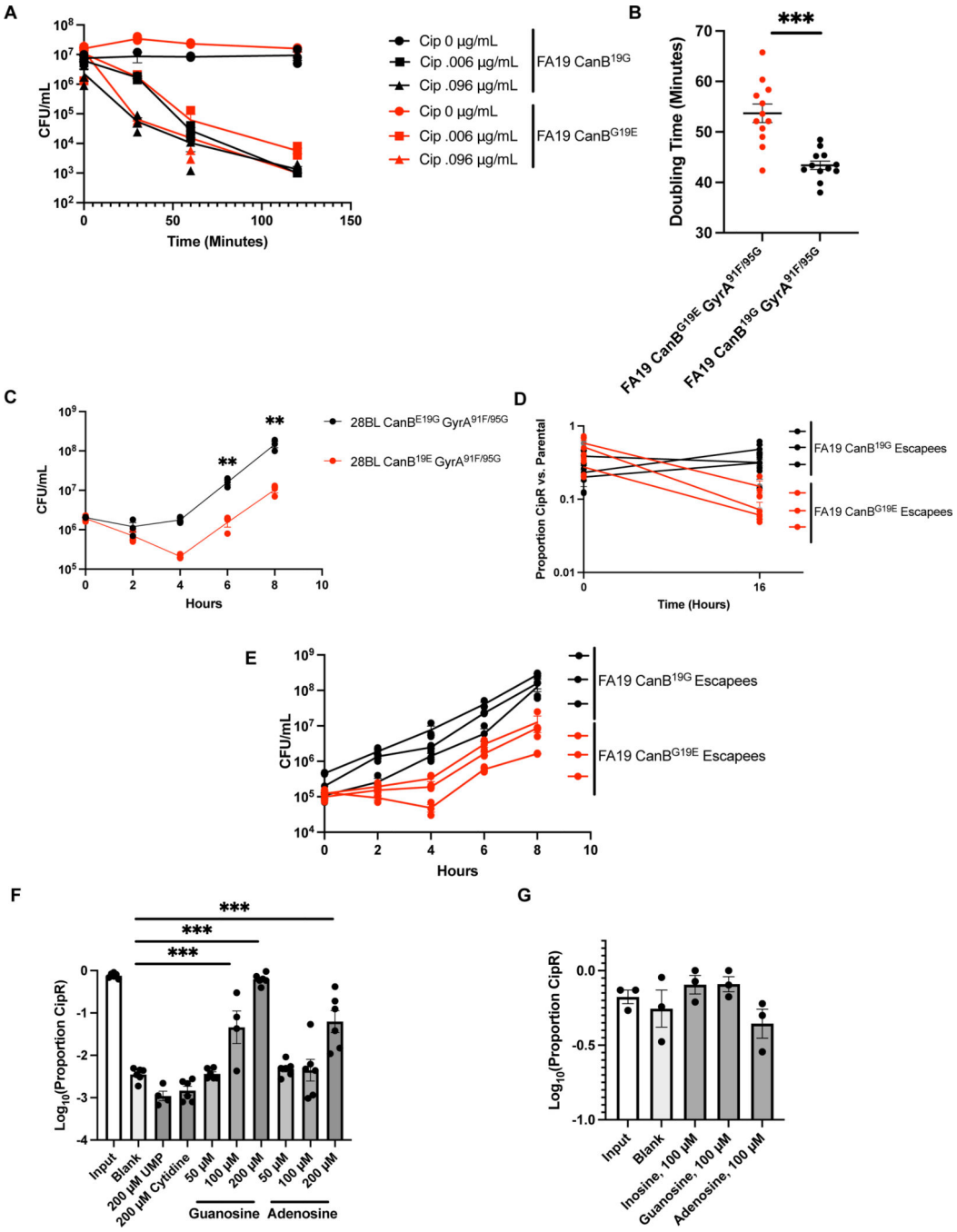

Extended Data Fig. 7.

The CanB^{19G} variant does not affect killing by ciprofloxacin, but CanB^{19G} provides an advantage in the presence of *gyrA* mutations across multiple *gyrA* alleles and strain backgrounds. **(A)** Kill curve of isogenic CanB FA19 at 2x MIC and 32x MIC (N=3, representative of two independent experiments). (**B**) Doubling time of replicates in Fig. 3E as determined by linear regression on log-transformed CFU/mL counts from 2–10 hours of growth (N=12, from two independent experiments, error bars represent SEM). Significance (p = 1.9e-5) by unpaired two-sided t-test. **(C)** Growth of CanB isogenic isogenic 28BL strains bearing ciprofloxacin resistance-determining GyrA$^{91F/95G}$ (N=3, representative of two independent experiments). Significance determined by unpaired two-sided t-test. **(D)** Competition between spontaneously ciprofloxacin resistant isogenic CanB strains (see Extended Data 2) and susceptible parental strains (N=3, representative of two independent experiments). **(E)** Growth curves of CanB isogenic FA19 strains with spontaneous ciprofloxacin resistance-determining *gyrA* alleles (N=3, representative of two independent experiments). **(F and G)** Competition between **(F)** FA19 CanB^{G19E} and FA19 CanB^{G19E} GyrA^{91F} (N=6, except UMP and 100 μM Adenosine, N=4) and **(G)** FA19 CanB^{19G} and FA19 CanB^{19G} GyrA^{91F} (N=3) after 16 hours along with media supplementation in liquid GCP-K (representative of two independent experiments, error bars represent SEM). Significance (from left to right, p = 0.0002, p = 5.7e-13, p = 3.86e-5), by oneway ANOVA with Dunnett's multiple comparisons test. *p<0.05, **p<0.01, ***p<0.001

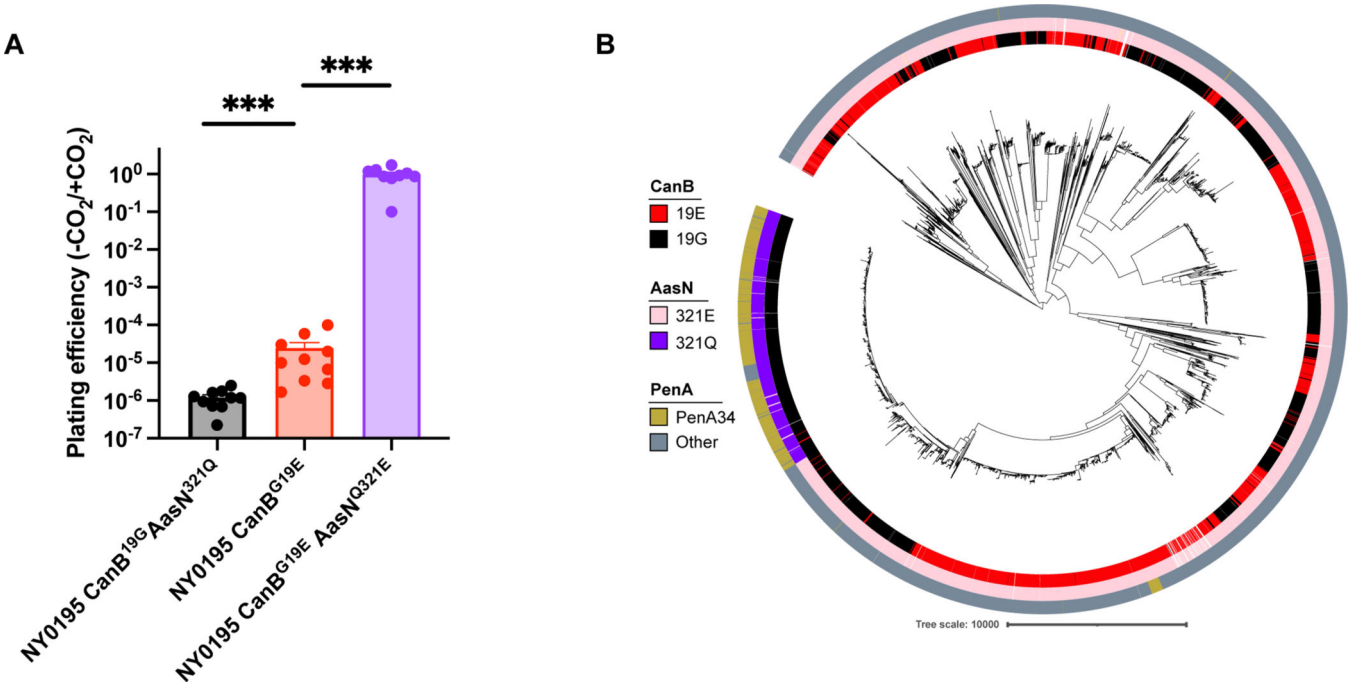

Extended Data Fig. 8.

(A) Plating efficiency in the absence and presence of supplemental CO_2 of clinical *N. gonorrhoeae* isolate NY0195 following the introduction of mutations in CanB and AasN (N=6, from two independent experiments, error bars represent SEM). Significance (from left to right, p = 0.00034 p = 0.00028) by two-sided Mann-Whitney U test. **(B)** Maximum-

likelihood tree as in Figure 1A overlaid with tracks indicating AasN allele and the ceftriaxone resistance determinant mosaic PenA34 allele. *p<0.05, **p<0.01, ***p<0.001

Supplementary Material

Refer to Web version on PubMed Central for supplementary material.

Acknowledgements

We thank the members of the Grad Lab and the Waldor lab for their invaluable feedback into this project; the members of the GC subgroup for their invaluable contributions, particularly Adi Bandekar; Sam Palace in particular for her thoughts on experimental design; and the Microbial Genome Sequencing Center (https://www.migscenter.com/) for their work sequencing strains. This work was supported by NIH R01 AI132606 and R01 AI153521 and by the Smith Family Foundation Odyssey award (YHG) and R01 AI 042347-24 (MKW). Authors are further funded by NIH F30 AI160911-01 (DHFR), NIH T32 GM007753 (DHFR), NIH F31 AI156949-01 (KH), and NIH T32 AI132120-01.

Data Availability

The datasets generated during and/or analyzed during the current study can be found in the source data associated with this work. RNA-seq reads are available publicly at SRA Bioproject PRJNA869861. The NCCP11945 genome is accessible via RefSeq accession NC_011035.1. Genomic data, metadata, and accession numbers are publicly available in previously published work.[68]

References

1. Rowley J. et al. Chlamydia, gonorrhoea, trichomoniasis and syphilis: global prevalence and incidence estimates, 2016. Bull World Health Organ 97, 548–562P (2019). 10.2471/BLT.18.228486 [PubMed: 31384073]
2. Marazzo JM & Apicella MA in Principles and Practice of Infectious Disease (eds Bennett JE, Dolin R, & Blaser MJ) Ch. 214, (Saunders, 2015).
3. Ma KC et al. Adaptation to the cervical environment is associated with increased antibiotic susceptibility in Neisseria gonorrhoeae. Nature communications 11, 4126 (2020). 10.1038/s41467-020-17980-1
4. Lewis LA & Ram S. Complement interactions with the pathogenic Neisseriae: clinical features, deficiency states, and evasion mechanisms. FEBS Lett 594, 2670–2694 (2020). 10.1002/1873-3468.13760 [PubMed: 32058583]
5. Golparian D. et al. Genomic evolution of Neisseria gonorrhoeae since the preantibiotic era (1928–2013): antimicrobial use/misuse selects for resistance and drives evolution. BMC genomics 21, 116 (2020). 10.1186/s12864-020-6511-6 [PubMed: 32013864]
6. Gransden WR, Warren CA, Phillips I, Hodges M. & Barlow D. Decreased susceptibility of Neisseria gonorrhoeae to ciprofloxacin. Lancet (London, England) 335, 51 (1990). 10.1016/0140-6736(90)90177-7
7. Unemo M. & Shafer WM Antimicrobial resistance in Neisseria gonorrhoeae in the 21st century: past, evolution, and future. Clinical microbiology reviews 27, 587–613 (2014). 10.1128/cmr.00010-14 [PubMed: 24982323]
8. CDC. Sexually Transmitted Disease Surveillance - 2020. (2020).
9. WHO. WHO Gonococcal AMR Surveillance Programme, <https://www.who.int/data/gho/data/themes/topics/who-gonococcal-amr-surveillance-programme-who-gasp> (2022).
10. Rubin DHF, Ross JDC & Grad YH The frontiers of addressing antibiotic resistance in Neisseria gonorrhoeae. Transl Res (2020). 10.1016/j.trsl.2020.02.002

11. Ito M. et al. Emergence and spread of Neisseria gonorrhoeae clinical isolates harboring mosaic-like structure of penicillin-binding protein 2 in Central Japan. Antimicrobial agents and chemotherapy 49, 137–143 (2005). 10.1128/aac.49.1.137-143.2005 [PubMed: 15616287]
12. Sánchez-Busó L. et al. The impact of antimicrobials on gonococcal evolution. Nature Microbiology 4, 1941–1950 (2019). 10.1038/s41564-019-0501-y
13. Mortimer TD et al. The Distribution and Spread of Susceptible and Resistant Neisseria gonorrhoeae Across Demographic Groups in a Major Metropolitan Center. Clinical infectious diseases : an official publication of the Infectious Diseases Society of America 73, e3146–e3155 (2021). 10.1093/cid/ciaa1229 [PubMed: 32829411]
14. Williamson DA et al. Bridging of Neisseria gonorrhoeae lineages across sexual networks in the HIV pre-exposure prophylaxis era. Nature communications 10, 3988 (2019). 10.1038/s41467-019-12053-4
15. Lopatkin AJ et al. Clinically relevant mutations in core metabolic genes confer antibiotic resistance. Science (New York, N.Y.) 371 (2021). 10.1126/science.aba0862
16. Pinheiro F, Warsi O, Andersson DI & Lässig M. Metabolic fitness landscapes predict the evolution of antibiotic resistance. Nat Ecol Evol 5, 677–687 (2021). 10.1038/s41559-021-01397-0 [PubMed: 33664488]
17. Spence JM, Wright L. & Clark VL Laboratory maintenance of Neisseria gonorrhoeae. Current protocols in microbiology Chapter 4, Unit 4A.1 (2008). 10.1002/9780471729259.mc04a01s8
18. Platt DJ Carbon dioxide requirement of Neisseria gonorrhoeae growing on a solid medium. J Clin Microbiol 4, 129–132 (1976). [PubMed: 823171]
19. Huang S. et al. Crystal structure of carbonic anhydrase from Neisseria gonorrhoeae and its complex with the inhibitor acetazolamide. J Mol Biol 283, 301–310 (1998). 10.1006/jmbi.1998.2077 [PubMed: 9761692]
20. Elleby B, Chirica LC, Tu C, Zeppezauer M. & Lindskog S. Characterization of carbonic anhydrase from Neisseria gonorrhoeae. Eur J Biochem 268, 1613–1619 (2001). [PubMed: 11248679]
21. Hewitt CS et al. Structure-Activity Relationship Studies of Acetazolamide-Based Carbonic Anhydrase Inhibitors with Activity against Neisseria gonorrhoeae. ACS Infect Dis 7, 1969–1984 (2021). 10.1021/acsinfecdis.1c00055 [PubMed: 33765392]
22. Remmele CW et al. Transcriptional landscape and essential genes of Neisseria gonorrhoeae. Nucleic acids research 42, 10579–10595 (2014). 10.1093/nar/gku762 [PubMed: 25143534]
23. Merlin C, Masters M, McAteer S. & Coulson A. Why is carbonic anhydrase essential to Escherichia coli? Journal of bacteriology 185, 6415–6424 (2003). 10.1128/jb.185.21.6415-6424.2003 [PubMed: 14563877]
24. Teufel F. et al. SignalP 6.0 predicts all five types of signal peptides using protein language models. Nature biotechnology (2022). 10.1038/s41587-021-01156-3
25. Jumper J. et al. Highly accurate protein structure prediction with AlphaFold. Nature 596, 583–589 (2021). 10.1038/s41586-021-03819-2 [PubMed: 34265844]
26. Burghout P. et al. A single amino acid substitution in the MurF UDP-MurNAc-pentapeptide synthetase renders Streptococcus pneumoniae dependent on CO2 and temperature. Molecular microbiology 89, 494–506 (2013). 10.1111/mmi.12292 [PubMed: 23750975]
27. Dillard JP Genetic Manipulation of Neisseria gonorrhoeae. Current protocols in microbiology 0 4, Unit4A.2 (2011). 10.1002/9780471729259.mc04a02s23
28. Tuttle DM & Scherp HW Studies on the carbon dioxide requirement of Neisseria meningitidis. Journal of bacteriology 64, 171–182 (1952). 10.1128/jb.64.2.171-182.1952 [PubMed: 14955510]
29. Fan SH et al. MpsAB is important for Staphylococcus aureus virulence and growth at atmospheric CO(2) levels. Nature communications 10, 3627 (2019). 10.1038/s41467-019-11547-5
30. Linhares IM, Summers PR, Larsen B, Giraldo PC & Witkin SS Contemporary perspectives on vaginal pH and lactobacilli. American journal of obstetrics and gynecology 204, 120.e121–125 (2011). 10.1016/j.ajog.2010.07.010
31. Muir A. et al. Construction of a complete set of Neisseria meningitidis mutants and its use for the phenotypic profiling of this human pathogen. Nature communications 11, 5541 (2020). 10.1038/s41467-020-19347-y

32. Kampmeier RH Introduction of sulfonamide therapy for gonorrhea. Sexually transmitted diseases 10, 81–84 (1983). 10.1097/00007435-198304000-00007 [PubMed: 6362039]
33. Zampieri M. et al. Metabolic constraints on the evolution of antibiotic resistance. Mol Syst Biol 13, 917 (2017). 10.15252/msb.20167028 [PubMed: 28265005]
34. Yao J, Bruhn DF, Frank MW, Lee RE & Rock CO Activation of Exogenous Fatty Acids to Acyl-Acyl Carrier Protein Cannot Bypass FabI Inhibition in Neisseria. The Journal of Biological Chemistry 291, 171–181 (2016). 10.1074/jbc.M115.699462 [PubMed: 26567338]
35. Kitzenberg DA et al. Adenosine Awakens Metabolism to Enhance Growth-Independent Killing of Tolerant and Persister Bacteria across Multiple Classes of Antibiotics. mBio 13, e0048022 (2022). 10.1128/mbio.00480-22
36. Firestine SM, Poon SW, Mueller EJ, Stubbe J. & Davisson VJ Reactions catalyzed by 5-aminoimidazole ribonucleotide carboxylases from Escherichia coli and Gallus gallus: a case for divergent catalytic mechanisms. Biochemistry 33, 11927–11934 (1994). 10.1021/bi00205a031 [PubMed: 7918411]
37. Andersson DI & Hughes D. Antibiotic resistance and its cost: is it possible to reverse resistance? Nature reviews. Microbiology 8, 260–271 (2010). 10.1038/nrmicro2319 [PubMed: 20208551]
38. MacLean RC & San Millan A. The evolution of antibiotic resistance. Science (New York, N.Y.) 365, 1082–1083 (2019). 10.1126/science.aax3879 [PubMed: 31515374]
39. Sousa A, Magalhães S. & Gordo I. Cost of antibiotic resistance and the geometry of adaptation. Mol Biol Evol 29, 1417–1428 (2012). 10.1093/molbev/msr302 [PubMed: 22144641]
40. Sommer MOA, Munck C, Toft-Kehler RV & Andersson DI Prediction of antibiotic resistance: time for a new preclinical paradigm? Nature reviews. Microbiology 15, 689–696 (2017). 10.1038/nrmicro.2017.75 [PubMed: 28757648]
41. Kohler PL, Hamilton HL, Cloud-Hansen K. & Dillard JP AtlA functions as a peptidoglycan lytic transglycosylase in the Neisseria gonorrhoeae type IV secretion system. Journal of bacteriology 189, 5421–5428 (2007). 10.1128/jb.00531-07 [PubMed: 17526702]
42. Ramsey ME, Hackett KT, Kotha C. & Dillard JP New complementation constructs for inducible and constitutive gene expression in Neisseria gonorrhoeae and Neisseria meningitidis. Appl Environ Microbiol 78, 3068–3078 (2012). 10.1128/aem.07871-11 [PubMed: 22327577]
43. Norrander J, Kempe T. & Messing J. Construction of improved M13 vectors using oligodeoxynucleotide-directed mutagenesis. Gene 26, 101–106 (1983). 10.1016/0378-1119(83)90040-9 [PubMed: 6323249]
44. Edwards RA, Keller LH & Schifferli DM Improved allelic exchange vectors and their use to analyze 987P fimbria gene expression. Gene 207, 149–157 (1998). 10.1016/s0378-1119(97)00619-7 [PubMed: 9511756]
45. Maness MJ & Sparling PF Multiple antibiotic resistance due to a single mutation in Neisseria gonorrhoeae. J Infect Dis 128, 321–330 (1973). 10.1093/infdis/128.3.321 [PubMed: 4269625]
46. Cohen MS et al. Human experimentation with Neisseria gonorrhoeae: rationale, methods, and implications for the biology of infection and vaccine development. J Infect Dis 169, 532–537 (1994). 10.1093/infdis/169.3.532 [PubMed: 8158024]
47. Faruki H. & Sparling PF Genetics of resistance in a non-beta-lactamase-producing gonococcus with relatively high-level penicillin resistance. Antimicrobial agents and chemotherapy 30, 856–860 (1986). 10.1128/aac.30.6.856 [PubMed: 3101587]
48. Johnson SR, Steiner BM & Perkins GH Cloning and characterization of the catalase gene of Neisseria gonorrhoeae: use of the gonococcus as a host organism for recombinant DNA. Infection and Immunity 64, 2627–2634 (1996). 10.1128/iai.64.7.2627-2634.1996 [PubMed: 8698488]
49. Guyer MS, Reed RR, Steitz JA & Low KB Identification of a sex-factor-affinity site in E. coli as gamma delta. Cold Spring Harb Symp Quant Biol 45 Pt 1, 135–140 (1981). 10.1101/sqb.1981.045.01.022 [PubMed: 6271456]
50. Palace SG et al. RNA polymerase mutations cause cephalosporin resistance in clinical Neisseria gonorrhoeae isolates. Elife 9 (2020). 10.7554/eLife.51407
51. Kellogg DS Jr., Peacock WL Jr., Deacon WE, Brown L. & Pirkle DI Neisseria Gonorrhoeae. I. Virulence Genetically Linked to Cloncal Variation. Journal of bacteriology 85, 1274–1279 (1963). 10.1128/jb.85.6.1274-1279.1963 [PubMed: 14047217]

52. Heng L. Aligning sequence reads, clone sequences and assembly contigs with BWA-MEM. arXiv (2013). https://doi.org:1303.3997
53. García-Alcalde F. et al. Qualimap: evaluating next-generation sequencing alignment data. Bioinformatics 28, 2678–2679 (2012). 10.1093/bioinformatics/bts503 [PubMed: 22914218]
54. Walker BJ et al. Pilon: an integrated tool for comprehensive microbial variant detection and genome assembly improvement. PLoS One 9, e112963 (2014). 10.1371/journal.pone.0112963 [PubMed: 25409509]
55. Bankevich A. et al. SPAdes: a new genome assembly algorithm and its applications to single-cell sequencing. J Comput Biol 19, 455–477 (2012). 10.1089/cmb.2012.0021 [PubMed: 22506599]
56. Seemann T. Prokka: rapid prokaryotic genome annotation. Bioinformatics 30, 2068–2069 (2014). 10.1093/bioinformatics/btu153 [PubMed: 24642063]
57. Page AJ et al. Roary: rapid large-scale prokaryote pan genome analysis. Bioinformatics 31, 3691–3693 (2015). 10.1093/bioinformatics/btv421 [PubMed: 26198102]
58. Thorpe HA, Bayliss SC, Sheppard SK & Feil EJ Piggy: a rapid, large-scale pangenome analysis tool for intergenic regions in bacteria. Gigascience 7, 1–11 (2018). 10.1093/gigascience/giy015
59. Croucher NJ et al. Rapid phylogenetic analysis of large samples of recombinant bacterial whole genome sequences using Gubbins. Nucleic acids research 43, e15 (2015). 10.1093/nar/gku1196 [PubMed: 25414349]
60. Letunic I. & Bork P. Interactive Tree Of Life (iTOL) v5: an online tool for phylogenetic tree display and annotation. Nucleic acids research 49, W293–w296 (2021). 10.1093/nar/gkab301 [PubMed: 33885785]
61. Lees JA, Galardini M, Bentley SD, Weiser JN & Corander J. pyseer: a comprehensive tool for microbial pangenome-wide association studies. Bioinformatics 34, 4310–4312 (2018). 10.1093/bioinformatics/bty539 [PubMed: 30535304]
62. Langmead B. & Salzberg SL Fast gapped-read alignment with Bowtie 2. Nat Methods 9, 357–359 (2012). 10.1038/nmeth.1923 [PubMed: 22388286]
63. Li H. A statistical framework for SNP calling, mutation discovery, association mapping and population genetical parameter estimation from sequencing data. Bioinformatics 27, 2987–2993 (2011). :10.1093/bioinformatics/btr509 [PubMed: 21903627]
64. Liao Y, Smyth GK & Shi W. featureCounts: an efficient general purpose program for assigning sequence reads to genomic features. Bioinformatics 30, 923–930 (2014). 10.1093/bioinformatics/btt656 [PubMed: 24227677]
65. Love MI, Huber W. & Anders S. Moderated estimation of fold change and dispersion for RNA-seq data with DESeq2. Genome Biol 15, 550 (2014). 10.1186/s13059-014-0550-8 [PubMed: 25516281]
66. Stein DC, Danaher RJ & Cook TM Characterization of a gyrB mutation responsible for low-level nalidixic acid resistance in Neisseria gonorrhoeae. Antimicrobial agents and chemotherapy 35, 622–626 (1991). 10.1128/aac.35.4.622 [PubMed: 1906260]
67. Bushnell B, Rood J. & Singer E. BBMerge - Accurate paired shotgun read merging via overlap. PloS one 12, e0185056 (2017). 10.1371/journal.pone.0185056 [PubMed: 29073143]
68. Ma KC et al. Increased antibiotic susceptibility in Neisseria gonorrhoeae through adaptation to the cervical environment. bioRxiv, 2020.2001.2007.896696 (2020). 10.1101/2020.01.07.896696
69. Stamatakis A. RAxML version 8: a tool for phylogenetic analysis and post-analysis of large phylogenies. Bioinformatics 30, 1312–1313 (2014). 10.1093/bioinformatics/btu033 [PubMed: 24451623]
70. Gibson DG et al. Enzymatic assembly of DNA molecules up to several hundred kilobases. Nat Methods 6, 343–345 (2009). 10.1038/nmeth.1318 [PubMed: 19363495]
71. Wade JJ & Graver MA A fully defined, clear and protein-free liquid medium permitting dense growth of Neisseria gonorrhoeae from very low inocula. FEMS microbiology letters 273, 35–37 (2007). 10.1111/j.1574-6968.2007.00776.x [PubMed: 17559396]
72. Mazoyer A, Drouilhet R, Despréaux S. & Ycart B. flan: An R Package for Inference on Mutation Models. R Journal 9, 334–351 (2017). 10.32614/RJ-2017-029

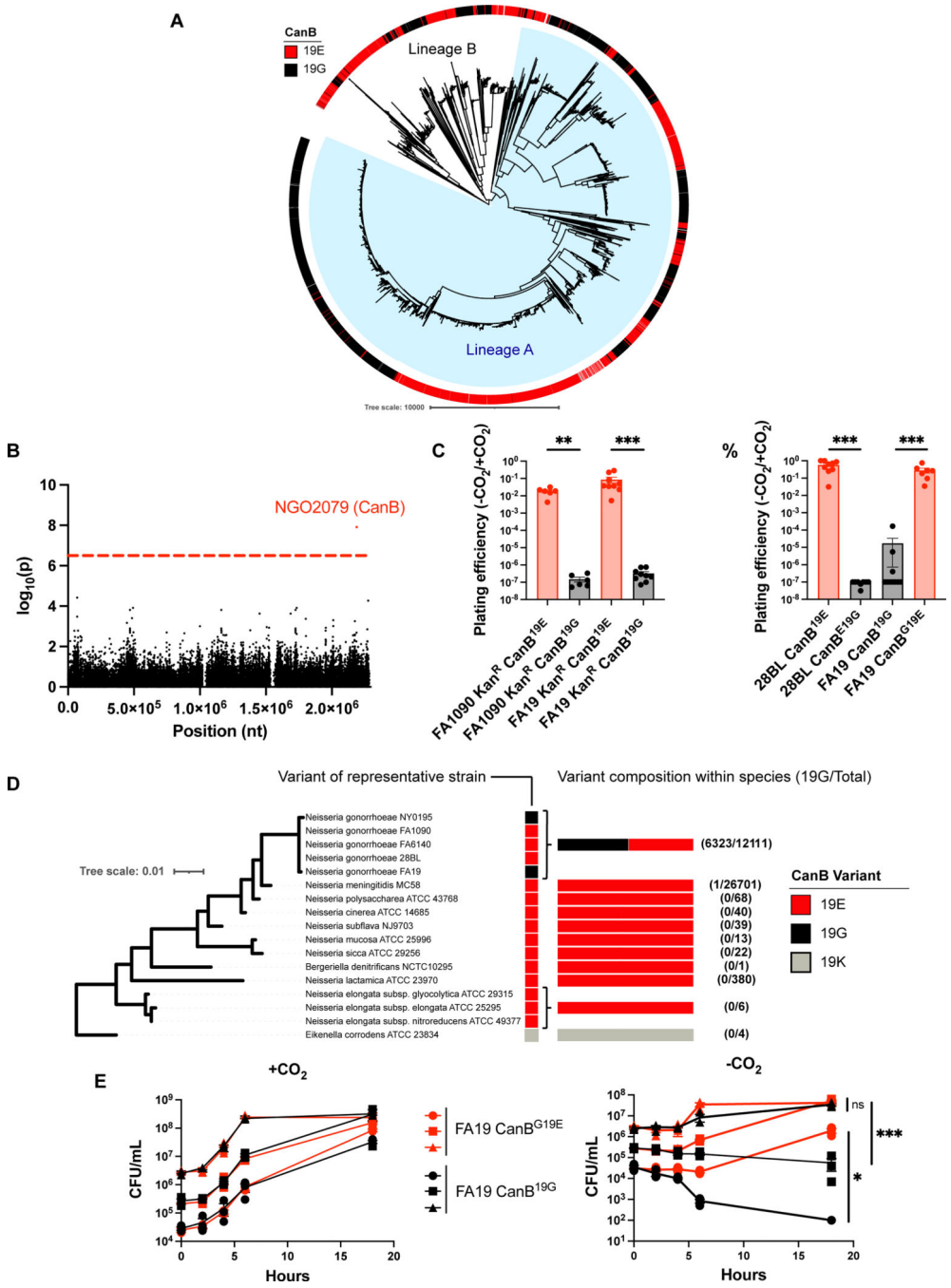

Figure 1.

A SNP in *ngo2079*, encoding a β-carbonic anhydrase, is necessary and sufficient to explain dependence on supplemental CO_2 in *N. gonorrhoeae*. **(A)** Maximum-likelihood phylogenetic tree of 5,007 strains of *N. gonorrhoeae* with a colored track representing CanB variant. Branch length represents total number of substitutions after removal of predicted recombinations. Lineage A represents isolates that arose phylogeographically After the introduction of *N. gonorrhoeae* into Asia, while Lineage B represents isolates that arose Before that breakpoint, as defined by Sánchez-Busó *et al.*[12] **(B)** Manhattan plot of SNPs

associated with dependence on supplemental CO_2 across 30 strains of *N. gonorrhoeae*. Dotted line represents a p-value of 0.05 with Bonferroni correction for 57,691 unitigs. **(C)** Plating efficiencies in the absence and presence of 5% supplemental CO_2 of CanB variants introduced by kanamycin co-selection in *N. gonorrhoeae* strains FA1090 (parental $CanB^{19E}$) and FA19 (parental $CanB^{19G}$) (From left to right, N = 6, 6, 9, 9, from two independent experiments, error bars represent SEM). Significance (from left to right, p = 0.00512, p = 0.00062) determined by two-sided Mann-Whitney U test. **(D)** Plating efficiencies as in (**C**) of *N. gonorrhoeae* strains 28BL (parental $CanB^{19E}$) and FA19 (parental $CanB^{19G}$) with isogenic CanB mutants (from left to right, N = 9, 8, 10, 7, from two independent experiments, error bars represent SEM). Significance (from left to right, p = 0.00062, p = 0.00076) determined by two-sided Mann-Whitney U test. **(E)** NGO2079/CanB variants across sequenced *Neisseria* and related species represented alongside a 16S maximum-likelihood tree. Branch length represents number of substitutions per site. **(F)** Growth of FA19 CanB isogenic strains in the presence and absence of supplemental CO_2 (N=3, representative of two independent experiments, error bars represent SEM). Significance (from top to bottom, p = 0.45, p = 0.00069, p = 0.014) at 18 hours determined by unpaired two-sided t-test. *p<0.05, **p<0.01, 599 ***p<0.001

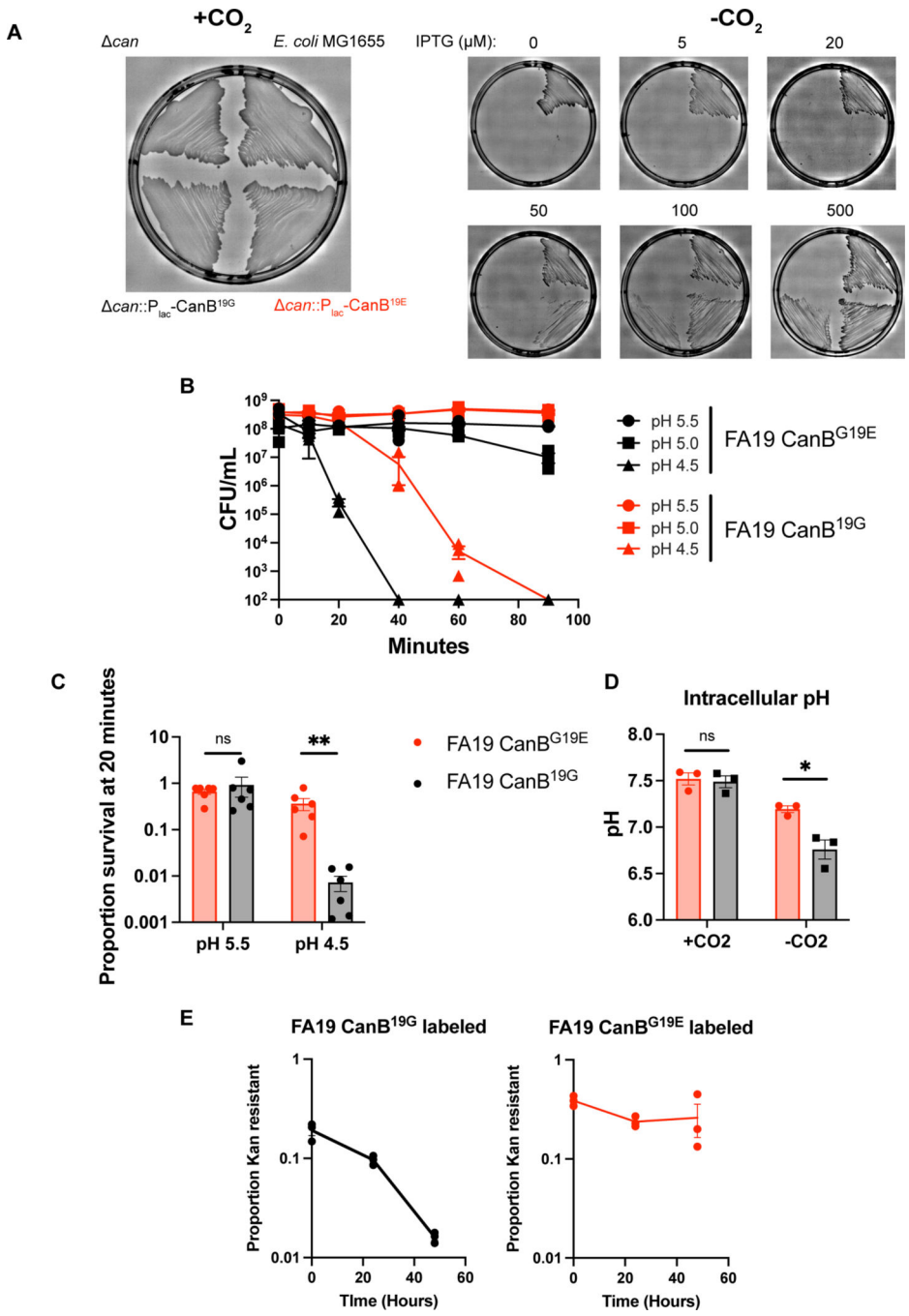

Figure 2.

The 19G variant of CanB is a functional hypomorph. **(A)** Growth of parental *E. coli* MG1655, MG1655Δ*can*, and MG1655Δ*can* complemented with CanB variants under different levels of induction. **(B)** Survival curve under multiple low pH conditions of FA19 isogenic CanB isolates in monoculture (N=3, representative of three independent experiments, error bars represent SEM). **(C)** As in (**B**), survival at 20 minutes of exposure to low pH conditions (N=6, from two independent experiments, error bars represent SEM). Significance (from left to right, p = 0.81, p = 0.002) by two-sided Mann-Whitney U test.

(D) Intracellular pH of FA19 CanB^{19G} and FA19 CanB^{G19E} as measured by flourimetric dye in the presence and absence of supplemental CO_2 (N=3, representative of two independent experiments, error bars represent SEM). Significance (p = 0.016) by unpaired two-sided t-test. **(E)** Competition under anaerobic conditions between FA19 isogenic CanB strains on GCB-K agar (N=3, representative of two independent experiments, error bars represent SEM). *p<0.05, **p<0.01, ***p<0.001

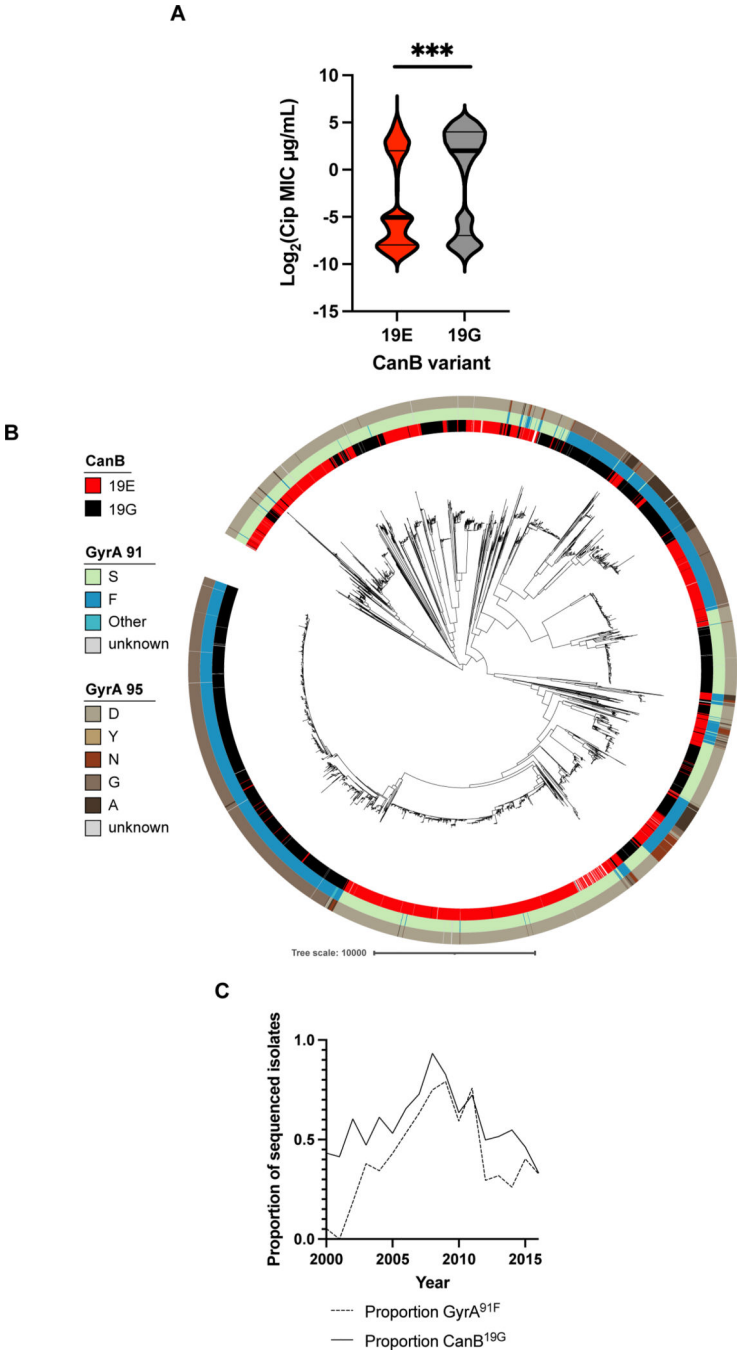

Figure 3.

The CanB^{19G} variant is associated with ciprofloxacin resistance **(A)** Violin plot of ciprofloxacin MICs for 8,912 *N. gonorrhoeae* clinical isolates. Thick lines represent median, thin lines represent 25th/75th percentiles. Significance (p = 1.3e-41) by two-sided Mann-Whitney U test. **(B)** Maximum-likelihood tree, as in Figure 1C, overlaid with tracks representing ciprofloxacin conferring variants of GyrA. **(C)** Proportion of sequenced U.S. isolates stratified by year that have the CanB^{19G} variant and the ciprofloxacin resistance-conferring GyrA^{91F} variant. *p<0.05, **p<0.01, ***p<0.001

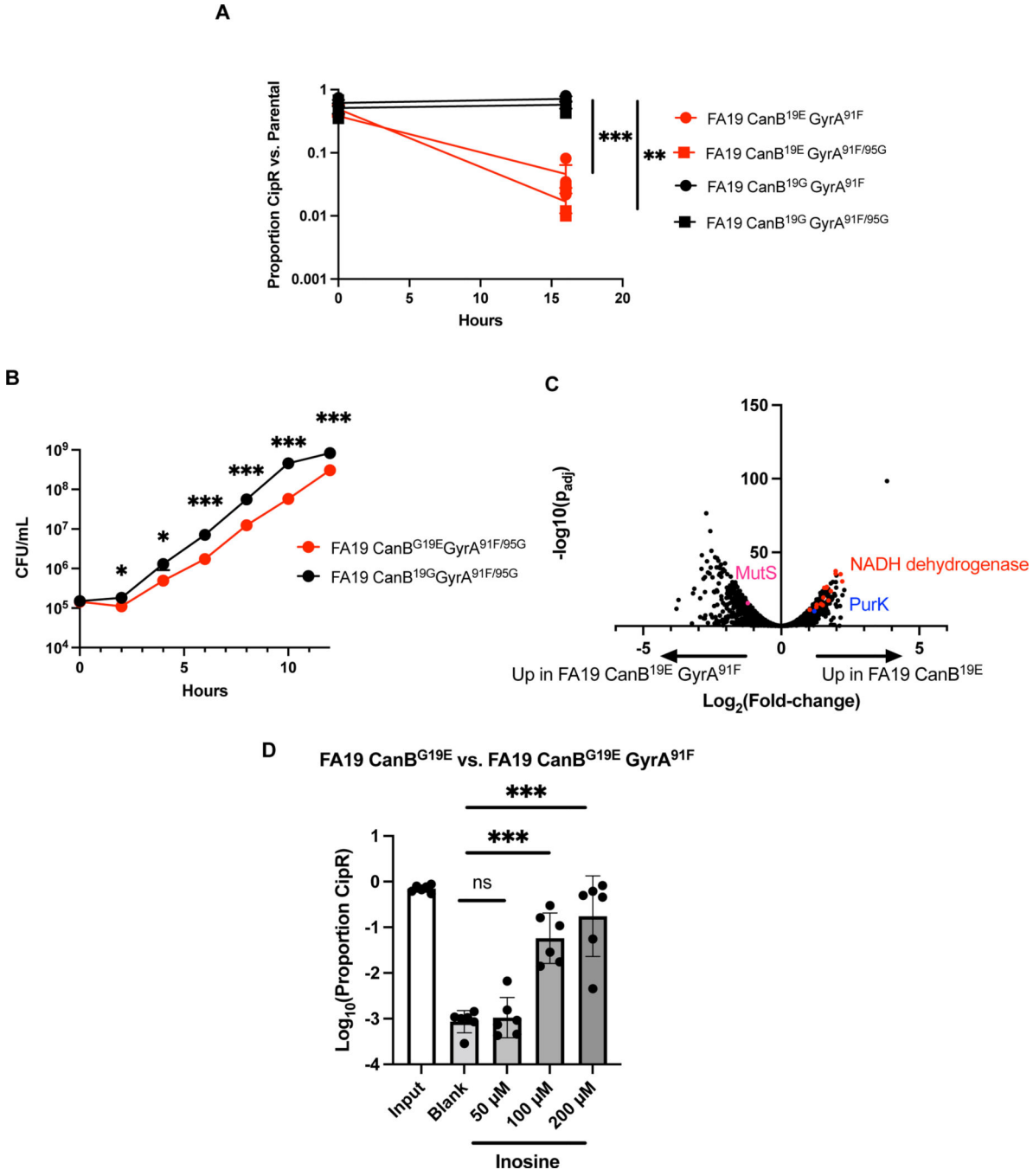

Figure 4.

CanB^{19G} provides a fitness advantage in the context of gyrase mutations. **(A)** Competition between ciprofloxacin resistant isogenic CanB strains and susceptible parental strains (N=3, representative of two independent experiments, error bars represent SEM). Significance (from left to right, p = 0.00063, p = 0.0019) by unpaired two-sided t-test. **(B)** Growth curves of CanB isogenic FA19 strains with ciprofloxacin resistance-determining *gyrA* alleles (N=12, data from two independent experiments, error bars represent SEM). Significance (from left to right, p = 0.018, 0.048, 5.0e-5, 9.7e-5, 0.00041, 0.00019) by unpaired two-

sided t-test. **(C)** Volcano plot of RNA-seq showing transcript levels compared between FA19 CanB^{G19E} and FA19 CanB^{G19E} GyrA^{91F} by DeSeq2. Specific transcripts of interest are highlighted in color. **(D)** Competition between FA19 CanB^{G19E} and FA19 CanB^{G19E} GyrA^{S91F} after 16 hours along with media supplementation in liquid GCP medium (N=6, representative of two independent experiments, error bars represent SEM). Significance (p = 0.99, p = 2.2e-6, p = 3.3e-9) by one-way ANOVA with Dunnett's multiple comparisons test. *p<0.05, **p<0.01, ***p<0.001